chemistry

MDPI

Review

Recent Advances on 2D Materials towards 3D Printing

I. Jénnifer Gómez [1,†], Nuria Alegret [2,†], Antonio Dominguez-Alfaro [3,*] and Manuel Vázquez Sulleiro [4,*]

1 Department of Condensed Matter Physics, Faculty of Science, Masaryk University, 61137 Brno, Czech Republic; gomez.perez@ceitec.muni.cz
2 CIC biomaGUNE, Basque Research and Technology Alliance (BRTA), 20014 Donostia-San Sebastián, Spain; nuria.alegret@ehu.eus
3 Faculty of Chemistry, University of Basque Country, Paseo Manuel Lardizabal 3, 20018 Donostia-San Sebastián, Spain
4 IMDEA Nanociencia, Ciudad Universitaria de Cantoblanco, Faraday 9, 28049 Madrid, Spain
* Correspondence: antoniodominguezalfaro@gmail.com (A.D.-A.); manuel.vazquez@imdea.org (M.V.S.)
† These authors contributed equally to the work.

Abstract: In recent years, 2D materials have been implemented in several applications due to their unique and unprecedented properties. Several examples can be named, from the very first, graphene, to transition-metal dichalcogenides (TMDs, e.g., MoS_2), two-dimensional inorganic compounds (MXenes), hexagonal boron nitride (h-BN), or black phosphorus (BP). On the other hand, the accessible and low-cost 3D printers and design software converted the 3D printing methods into affordable fabrication tools worldwide. The implementation of this technique for the preparation of new composites based on 2D materials provides an excellent platform for next-generation technologies. This review focuses on the recent advances of 3D printing of the 2D materials family and its applications; the newly created printed materials demonstrated significant advances in sensors, biomedical, and electrical applications.

Keywords: 2D materials; 3D printing; graphene; mxenes; TMDCs; MoS_2; black phosphorous; boron nitride

Citation: Gómez, I.J.; Alegret, N.; Dominguez-Alfaro, A.; Vázquez Sulleiro, M. Recent Advances on 2D Materials towards 3D Printing. *Chemistry* **2021**, *3*, 1314–1343. https://doi.org/10.3390/chemistry3040095

Academic Editors: Xiaoyan Zhang and Raul Arenal

Received: 30 September 2021
Accepted: 3 November 2021
Published: 6 November 2021

1. Introduction of 2D Materials

The curiosity about 2D materials started with the discovery of graphene in 2004 [1]. Since then, many other members have been included in this broad family of nanomaterials (e.g., TMDs, Mxenes, BP, or h-BN explained below) [2–9]. These layered materials can be obtained with several methods depending on the selected approach [3,10–13]. The general properties of 2D materials illustrated great potential for their use in printed composites, due to their atomic thickness, mechanical flexibility, transparency, and electrical conductivity. A general representation of them is presented in Figure 1.

Graphene is the most known allotrope of carbon. It consists of a single atomic layer of sp^2 hybridized carbon atoms in a honeycomb 2D structure. The properties of graphene are extraordinary, such as its mechanical strength, good flexibility, high thermal conductivity, high carrier density, and optical transparency [14–18]. Besides, many studies showed the capacity of graphene to introduce several moieties onto the surface through its functionalization, a valuable condition to adapt the material to the desired application and enhance the cohesion in their use as new-generation composites [19,20]. The biochemical properties of graphene are also unique: it presents antibacterial properties and high resistance toward a broad spectrum of chemicals, such as strong acids or bases, reductants, or oxidants [21,22]. The main industrial method for the fast and economical production of this material is its obtention from graphite through liquid phase exfoliation (LPE); this allows the lamination of the flakes having a few-layer material (<10) [23]. Other methods, where the chemical composition of the material is partially changed, can be obtained through oxidative intercalation (Graphene Oxide, GO) and its partial structural restoration via chemical

reduction (reduced Graphene Oxide, rGO), and having a material easy to handle, water dispersible [24–27], and commonly used in bio-applications. Bottom-up approaches based on the growth of synthetized individual flakes (e.g., chemical vapor deposition, CVD) usually have cost-effectiveness and scalability issues, depending on the application [22].

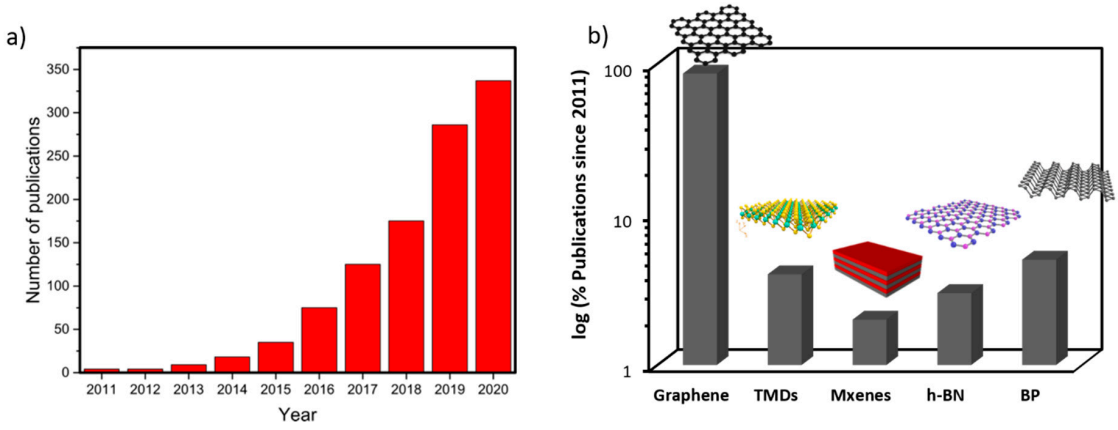

Figure 1. Statistics bibliography research by Web of Science: (**a**) Number of publications per year under the topics: 3D printing combined with 2D materials, Graphene, Mxenes, TMDCs, MoS_2, Black phosphorous, Boron nitride and (**b**) Relative percentage of publications since 2010 per 2D material in the 3D printing field.

TMDs are a group of compounds formed by a transition metal and an element group VI, chalcogenides, generally represented as MX_2 formula, where the M (Mo, W, etc.) atoms are arranged in one plane surrounded by two other planes of X through a covalent bond. These 3-plane distributions can vary, obtaining structures with tetragonal (T), hexagonal (H), or octahedral units changing their properties from metallic to semiconductor in most TMDs [28]. These materials have very particular characteristics of interest in nanotechnology and energy conversion. They are often very tough, stable, have high charge mobility, and can absorb and emit (fluorescence) large amounts of light. Due to quantum confinement, exfoliating semiconducting TMDs have layer-dependent bandgaps, which make these materials suitable for optoelectronics and photodetectors [29]. Among all TMDs, molybdenum disulfide (MoS_2) can be found in nature as molybdenite. It is only 6.5 Å thick and is often used as a representative TMD [30]. Several methods are viable for obtaining MoS_2, or graphene. LPE is the most commonly used in obtaining scalable quantities of the material. There are two main routes of LPE: chemical exfoliation, where atomic intercalation plays an essential role [31], and mechanical means, such as sonication [32–34].

A decade after their first appearance [35], Mxenes are a vast family of 2D materials consisting of a single layer of transition carbides, nitrides, or carbonides with the $M_{n+1}X_nT_x$ formula, where M refers to a transition metal (Ti, Mo, Cr, Nb, V, Sc, Zr, Hf or Ta), X stands for carbon or nitrogen, and T_x is a surface termination (fluorine, oxygen or hydroxyl) [36,37]. Due to the composition of these materials and the surface terminations, Mxenes have good hydrophilicity and significant influence on the Fermi level density of states, having interesting electronic properties [38,39]. Mxenes have been used as electrode materials for energy storage applications [40,41], biomedicine [42], photocatalysis [43], and other areas [44–46]. The production of mxenes is typically synthesized by top-down etching processes [47]. The exfoliation of these materials occurs through the etching of the MAX phase using strong etching solutions such as hydrochloric acid, lithium fluoride, or hydrofluoric acid [47].

Black phosphorus (BP) was first synthesized in 1914 by Percy W Bridgman by heating white phosphorus at high pressures. BP can be considered as a rare allotrope of phosphorus and consists of bidimensional phosphorous layers called phosphorene. The direct bandgap of the 2D black phosphorus makes an ideal candidate for optoelectronic applications; it presents a distinctive wrinkled structure and high-hole mobility with excellent mechanical, electrical, and optical properties [48]. The poor stability and easy chemical degradation through oxidation limits its use in many fields. However, in recent years people have fo-

cused on their use in energy storage devices, such as in batteries and supercapacitors [7,49], photocatalyst [50,51], biomedical applications [52], and sensors [53]. The synthesis methods are dominated by vapor-phase growth or liquid phase exfoliation; one of the most interesting methods is its obtention from the conversion of red phosphorous [54–56].

Hexagonal Boron Nitride (h-BN) consists of an equal number of arranged boron and nitrogen atoms in a 2D plane bonded via sp^2, forming a honeycomb structure [57]. The hexagonal layer of this material is similar to graphite and was broadly used as a lubricant [58,59]. h-BN is a thermally conductive material and electrical insulator; these properties turn this material into a screening substrate for other 2D materials in electronics, acting as an encapsulator [60]. h-BN is near-transparent with wide bandgap, thermally and chemically stable; in industry, BN has been used in cosmetics, insulation, lubrication, and others areas [59]. Diverse top-down exfoliation methods and bottom-up approaches have been utilized to produce BN nanosheets, using similar strategies mentioned above on other 2D materials [59,61–64].

Interest in 2D materials has been growing, and after their in-depth fundamental study, they have been incorporated into multiple applications, something similar to what happened with carbon nanotubes. In many cases, it has not been a complete replacement, but rather a combination with an application already known to enhance its properties. The compatibility of 2D materials and 3D printing is one example. Figure 1a shows how the interest is growing, and this is reflected in the number of publications that are achieved year after year. The unique properties of 2D materials, coupled with their incorporation into printing matrices, create a new generation of composites with combined properties used in various fields, which we will discuss below.

2. Methods of 3D Printing

3D printing allows the manufacturing of complex and functional architectures that are not feasible to produce using other approaches, such as curves, spheres, or intricate angles [65]. In particular, the 3D printing of 2D materials provides the advantages of architecture modularity and, at the same time, that contribute the intrinsic properties of the 2D material. Moreover, the use of 2D materials for 3D printing is a field that remains remarkably unexplored. Among the different materials cited, graphene and MXenes are the most used for the different methods. As well as for other materials, the most common methods utilized for 3D printing of 2D materials are direct ink writing (DIW) and fused deposition modeling (FDM) for extrusion-based printing, stereolithography (SLA), and digital light printing (DLP) for light-based printing and inkjet printing. However, besides these aforementioned direct-printing methods, few examples of coating printed structures with 2D material in a post-processing step are described [66].

A typical ink formulated for the printing of 2D material is composed mainly of three components: the target 2D material, a suitable solvent that disperses the mixture homogeneously, and the binder, which generally is a polymer. Besides, two parameters are critical for the printability of the ink: mechanical strength that holds the structure during the deposition and rheological parameters, such as surface tension, viscosity, and density that assist the process [66]. In Table 1, we have summarized some compositions and viscosities reported for printing throughout the different 3D printing methods.

Table 1. Typical compositions and viscosity properties of inks for general printing technologies. Values adapted with permission from ref. [67]. Copyright 2020 American Chemical Society and ref. [68]. Copyright 2020 RSC and under Creative Commons Attribution-Noncommercial.

Wet Ink Composition (wt%)					Viscosity (mPa·s)
Method	**Binder**	**Additive**	**Solvent**	**Pigment**	
Inkjet Printing	5–20	1–5	65–95	5–10	<100
Extrusion-based printing	40–60	1–5	25–45	12–17	<10,000
Light-based Printing	-	-	-	-	10–5000

2.1. Extrusion-Based Printing

Direct ink writing (DIW) and fused deposition modeling (FDM) are considered extrusion-based printing. The material, placed in a cartridge, is driven by different actions such as air, piston, or screw to the nozzle where it is deposited layer by layer with the desired shape (see Figure 2a, top). The main difference between both techniques is the way to feed the material. While DIW requires a specific ink with a more sensible rheological property, FDM uses a filament that is heated and deposited in a semi-molten state, driven by rollers [66].

Generally, DIW requires inks with high viscosity values (<10,000 Pa·s), but the optimal flow depends on the method that drives the material, i.e., action driven mechanically as a piston could move higher viscosities than driven air. If the viscosity is not enough to retain the desired shape after printing, the structure would collapse and break the continuity. Moreover, the conical, convergent or flat shape of the nozzle could change the transport mechanism providing unique properties, such as the alignment of the nanosheets or nanotubes [67,69]. Therefore, besides the ink properties, fidelity and resolution can be ensured by modulating specific parameters of the printing and extrusion rate, needle diameter, printed head speed, extrude material viscosity, and nozzle temperature [68,70]. Moreover, this method might require additional post-fabrication steps where the solvent is removed or the material recombined throughout sintering processes.

On the other hand, FDM is mainly commanded by thermoplastic polymers such as polycarbonate (PC), polylactic acid (PLA), acrylonitrile butadiene co-polymers (ABS), thermoplastic polyurethane (TPU), polyphenyl sulphone (PPSF), and polyvinyl alcohol (PVA). They have in common low melting temperatures and the easy crystallization processes, whereas the main drawback of this method is resolution and quality it that could be overcome by incorporating high aspect-ratio nanofillers that enhance the filament extrusion [71].

Poly (vinyl alcohol) (PVA) was formulated with BN nanosheets as ink for the DIW 3D printing of the thermal regulation textile. DMSO was used as a solvent to disperse the BN nanosheets uniformly in the polymer matrix. The printer used temperatures around 200 °C to make the polymer fluidic and deposit the boron-based material. Besides, PVA polymer confers crystallinity deposition, uniform dispersion, and high alignment of BN nanosheets that results in excellent mechanical strength (355 MPa) and, moreover, alignment affect to uniform heat dispersion and high thermal conductivity fibers [71,72].

Guiney et al. [73] have also proposed a printable hexagonal boron nitride (h-BN) using polylactide-*co*-glycolide (PLGA) as a polymer for the suitable ink (see Figure 2a, bottom). This combination required a tri-solvent system; ethylene glycol monobutyl ether (EGBE) worked as a surfactant to help the dispersion of h-BN particles, dichloromethane (DCM) was used to dissolve the PLGA, and di-butyl phthalate (DBP) was added as a plasticizer. Interestingly, during the extrusion process, DCM evaporated rapidly, making PLGA precipitated and condensed around h-BN particles forming a self-supporting structure.

BP nanosheets were polymerized with polypyrrole (PPy) to form a hybrid composite used for high-performance supercapacitor (SC) electrodes, with a specific capacitance up to 417 $F \cdot g^{-1}$. PEO-PPO-PEO copolymer was used as a plasticizer displaying an excellent viscoelastic flow and control of the rheology. The hybrid PPy/BP embedded in the polymer present excellent flow at temperatures below 0 °C, suitable DIW printing driven by a combination of syringe and air [74].

MXene-based inks have also been used for extrusion-based printing (see Figure 2a, bottom). Zhang et al. [75] presented an additive-free ink of 2D titanium carbide (Ti_3C_2Tx). The negative charge on the Ti_3C_2Tx nanosheets lead to a homogeneous dispersion without additives, such as polymer stabilizers or surfactants. The concentrated dispersions (≈36 mg mL^{-1}) exhibited good printing viscosity of ~0.71 Pa·s. They were used for the 2D inkjet printing and 3D extrusion printing of specific shaped patterns tested for super micro-capacitors.

A tailored poly(N-isopropylacrylamide-*co*-acrylamide-*co*-2-mercaptoethylacrylamide) (PNAM) was designed to conjugate with MoS_2 nanoparticles throughout thiol-activated chemistry. MoS_2/PNAM was 3D printed using a screw-drive printing head. The PNAM

was used as a plasticizer due to its suitable low initial viscosity (≈3.20 Pa·s) and shear-thinning behavior. Upon NIR exposure, MoS_2 acts as a cross-linker agent connecting polymeric-nanomaterial via click chemistry [76].

3D hybrid MoS_2/rGO aerogels were printed by extrusion printing driven by air pressure. Graphene oxide (GO) nanoflakes dispersed in deionized water were used as precursor ink. In this method, the base of the printing was set at −30 °C. It allows droplets to rapidly freeze into ice crystals. After the printing, the aerogel was then thermally annealed to produce the MoS_2-rGO hybrid aerogel characterized by its black-grey appearance [77]. This technique was used to create GO aerogel. Therefore, concentrate GO sheets were assembly in sheets when are freeze-drying forming aerogels. 3D GO ice templated aerogel was obtained by subsequent drying process for 48 h. After thermal annealing at 1000 °C, reduced GO (rGO) was finally obtained. Moreover, the growth of ice crystal during freeze casting forms π–π interaction between GO sheets and the aligned sheets [78].

Besides these 2D materials, Compton and Lewis created an epoxy ink with nano clay platelets solubilized in dimethyl methylphosphonate performing as additive/solvent that improves the rheological features and allow the printability [66].

Apart from the DIW examples, 2D materials such as MoS_2, WS_2, and three-dimensional (3D) graphite were infused in thermoplastic polymer matrices to form filaments suitable for the FDM method. Acrylonitrile butadiene styrene (ABS) and polyethylene terephthalate glycol (PETG) were used. To incorporate the 2D material to the polymer matrix, the fillers were dispersed in different weight percentages in the polymer and then they were spun forming a filament using Filabot spooler [79].

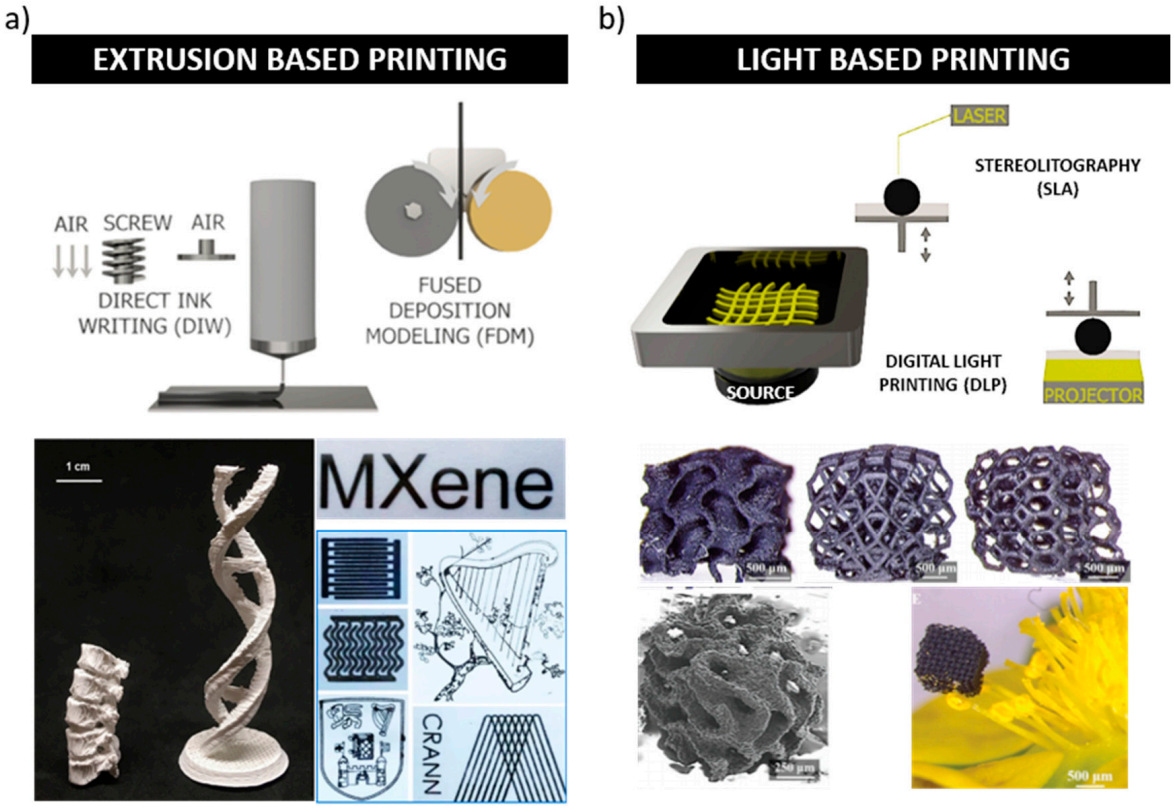

Figure 2. 3D printing methods used for 2D materials. (**a**) Extrusion-based printing shows the two methods described below, DIW, where the ink is impulse by different inputs (air, screw, or piston), and FDM, where a filament melted by temperature is deposited in the plate. Moreover, two examples are shown: hexagonal boron nitride dispersed in poly (lactic-co-glycolic acid) and printed by DIW (bottom left) and titanium carbide (Ti_3C_2Tx) MXene inks, dispersed in water in the absence of any additive for extrusion printing. (bottom right). Reprinted with permission from ref. [73] and ref. [75]. Copyright 2018

American Chemical Society and Creative Commons Attribution 4.0 Springer Nature, respectively. (**b**) Light based printing shows the methods described below, DLP where the light is made by projection and each slide of the structure, and it is photo-polymerized at the bottom of the platform and SLA where a laser source beam point-by-point on the top of the ink and forms the 3D structure. Figure adapted and reprinted with permission from ref. [80]. Copyright 2018 RSC and under Creative Commons Attribution-Noncommercial.

2.2. Light Based Printing

On the opposite of the liquid deposition methods, light-based printing is ruled by photopolymerization reactions with pre-polymers or monomers in a liquid state. There are two methods explored in this category: stereolithography (SLA) and digital light printing (DLP). Their main differences reside in the light source and how its contact with the liquid. In DLP, the light uses a digital micromirror device (DMD) that projects slide by slide the structure, while SLA uses a laser source that photocure point-by-point the design from the top (see Figure 2b, top). Besides these two methods, selective laser sintering (SLS) and two-photon lithography (TPL) can be considered light-based printing methods [71].

In light-based methods, viscosity is not a dramatical dependence parameter. Nevertheless, materials with high light absorption might produce problems in the layer-by-layer photopolymerization process.

Cross-linked GO sheets were dispersed 12 wt% photo-curable acrylates in NMP, using 2–4 wt% photo-initiator to generate a suitable ink for SLA printing (see Figure 2b, bottom). They demonstrated that complex and hierarchical 3D architectures of interconnected graphene sheets could be manufactured using this technique. Moreover, they showed that cross-linked graphene helps the formation of a porous structure thanks to the formation of a larger surface area. On the opposite, designs made by neat GO sheets did not show the same performance [80].

Graphene dispersed within polyaniline (PANI) nanofibers were mixed with poly acrylate resin solution to obtain a suitable ink for DLP. Furthermore, Sunghun Cho and co-workers incorporate polyurethanes in the mixture system, improving printing resolution by DLP method and getting higher tensile strength materials with superior conductivity than pristine materials [81,82].

2.3. Inkjet Printing

The inkjet printing (IKP) concept is similar to desktop printers that generally produce bi-dimensional shapes. In contrast with extrusion-based printing, the IKP printer requires an actuator head ruled by thermal, electric, magnetic, and piezoelectric actuators, which forces the ink to move out of the nozzle (see Figure 3a, top). Aerosol jet printing is also included in the IKP method, which uses an inert carrier gas flowing through the nanoparticle ink, forming an aerosol-nebulized ink droplet. The gas flow coupled with rapid solvent evaporation creates a very thin stream of particles that is patterned onto the substrate by a digitally-controlled precision gantry.

This control gives more precision in terms of droplet shape control. However, this technique is limited for Newtonian inks with viscosities lower than 100 mPa·s. The viscosity value is not only an essential parameter for avoiding the clogging of the nozzle, but also for the adhesion of the droplets [66,69].

IKP assisted by electrospray method was used to prepare 1T-MoS_2 structures. The ink was composed of 3D crumpled MoS_2 dispersed in water and using 2-butanol as an additive. Volatile solvents allow extremely fast evaporation, and subsequently, solidification guarantees a high proportion of the 1T phase. Besides, 1T c-MoS_2 inks and reduced graphene oxide (rGO) were also precisely printed with an interdigitated pattern. The aggregation-resistant properties of the 3D crumpled are ideal for anti-clogging disadvantages [83].

Silvestri and coworkers have recently developed a graphene-based bio-responsive and electroactive ink with a specific viscosity of 2.14 mPa·s, suitable for IKP. The graphene was conjugated with glucose oxidase and phthalocyanine and used for the detection of glucose, lactate, and primary alcohols [84].

In other work, PEDOT:PSS as the stabilizer of MoS_2 synthesized via one-pot hydrothermal method was used as ink (see Figure 3a, bottom) [85]. PEDOT:PSS as additive inhibited the aggregation of MoS_2. Furthermore, the interaction of both materials promoted the formation of the hydrogel by electrostatic interactions. Therefore, this gelation transition was used for printing specific shapes with great potential in a vast number of applications [86]. Ti_3C_2Tx Mxene prepared by selective etching of Al layers from Ti_3AlC_2 MAX powder with HF/HCl acidic combination was also formulated with PEG-diacrylate and commercial photo-initiator for aerosol printing [86].

2.4. Post-Functionalization Method

A method that has been used extensively is the functionalization with the 2D material after the 3D printing with one of the techniques described (see Figure 3b). In a pioneer work, Foster et al. [87] developed electrodes using a commercial graphene/PLA filament as the material source, consisting of 8 wt% of graphene and 92 wt% of PLA. Recently, Pumera and co-workers have carried out several examples of the manufacturing of electrodes using commercial conductive graphene/PLA filament for different electrochemical and sensing applications. They present two post-functionalization methods based on dip and spray coating. PLA post-functionalization allows binder-free coating throughout physisorption on the 3D-printed material. Furthermore, this represents a very simple and versatile method that was expanded to other 2D materials like MoS_2, $MoSe_2$, WS_2, and Wse_2 [88,89]. As well as solution coatings, the thick layer of molybdenum sulfide MoSx could be coated on the surface of the same printed PLA/graphene structures using electrodeposition methods [90–92].

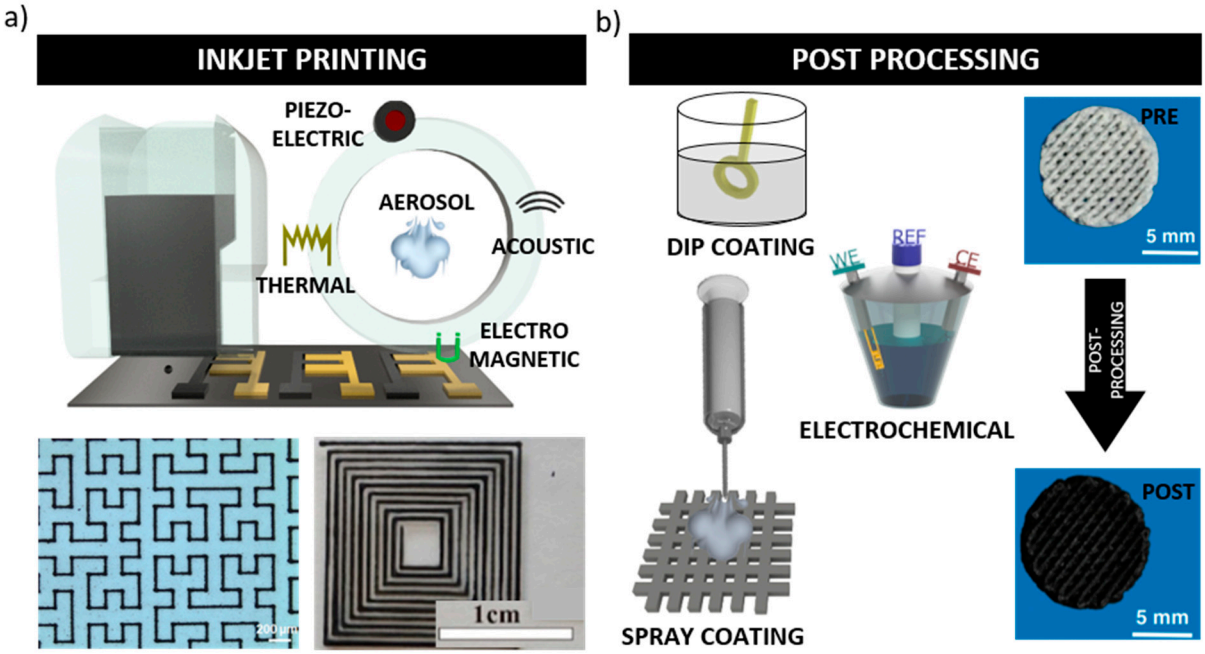

Figure 3. 3D printing methods used for 2D materials. (**a**) Inkjet printing, which uses the inputs as piezoelectric to forms droplets that are deposited on the surface. Two examples are shown: Ti_3C_2Tx MXene formulated with PEG-diacrylate for aerosol printing (bottom left) and PEDOT: PSS/MoS_2 patters printed by inkjet printing used for high-performance supercapacitors (bottom right). Reprinted with permission from ref. [83], ref. [85] and ref. [86]. Copyright 2021 American Chemical Society and 2020 Elsevier, respectively. (**b**) Post processing of previously printed 3D structures throughout electrochemical, dip, and spray coating with the targeted 2D material. Blue back images: three-dimensional (3D) with a MoS_2 hydrothermally incorporated at 180 °C using MoO_4^{2-} as precursor. Figure adapted and reprinted with permission from ref. [93]. Copyright 2017 Springer Nature under Creative Commons.

Scaffolds containing Ca^{-}, Mg^{-}, and Si^{-} bio-ceramic were used as a matrix material for MoS_2 nanosheets functionalization. Moreover, the material adhesion included combining it with a hydrothermal treatment of MoO_4^{-} used as precursor at 180 °C to then generate an ultrathin MoS_2 layer on top of the surface endowing them with photo-thermal therapeutic potential (see Figure 3b) [93].

A scaffold manufactured with MoS_2-PLGA was covered with borosilicate bioactive glass (BG) for photothermal therapy (PTT). Three different concentrations of MoS_2 nanosheets were integrated into 10% m/v PLGA solutions. The coating and drying procedure was repeated three times; then, the obtained scaffolds were washed with water and dried for 24 h at 60 °C, achieving hybrids MoS_2-PLGA film on the surface of the scaffolds [94].

Besides, Ti_3C_2Tx niobium carbide (Nb_2C) MXene was blended with bio-glass and formulated for printing. The bio-glass powder was added into 11 wt% PVA solution forming a cream-like consistency paste suitable for printing. Then, after drying at 1060 °C, the scaffold was obtained. The MXene nanomaterial was included in a post-processing step. The scaffold was soaked in Nb_2C@SiR solubilized in ethyl alcohol solution. Final BG@NbSiR scaffolds were obtained after solvent volatilized at room temperature [95].

As well, 2D Ti_3C_2Tx MXene ink was used to form paper substrates structures. PLA stamps were printed by FDM method and post-processed with the two dimensional ink by dip coating [71].

3. Applications

The unique and often tunable properties of 2D materials combined with technological advances, such as additive manufacturing (AM), commonly known as three-dimensional (3D) printing, has played a crucial role to fabricate a wide range of engineering component in many fields. Thus, they can serve as the active sensing element or a supporting substrate for diverse applications. In the last years, the demand for the designed and miniaturized systems appears to be a must (See Figure 1a). In this part of the review, a summary of several applications is presented.

3.1. Sensors

One of the most important applications of 2D materials lies in the field of sensors due to their unique optoelectronic and mechanical properties as well the large specific surface area [96]. Overall, 3D-printed sensors combined with 2D materials can be roughed classify into the following major types: biosensors, chemical, and physical sensors.

3.1.1. Biosensors

Due to technological advances, sensors have found their place in several aspects of human life. The recognition and detection of proteins, enzymes, antibodies, and other biomolecules is a high biological, technological, and pharmaceutical importance task. For this purpose, 3D-printed sensors based on 2D materials have proven to be an excellent choice because of their simple and unique processing and often tunable properties. In this regard, graphene appears to be a promising carrier platform for the biological recognition of glucose in actual samples [97]. Zhang and coworkers prepared an ultrasensitive non-enzymatic glucose biosensor by a facile screen-printing method. In detail, the graphite electrodes were modified by a micro flower structure from copper oxide/few-layer graphene, and its incorporation significantly improved the performance of the fabricated glucose sensors. The fabricated sensors could avoid the interferents from real samples, such as dopamine, ascorbic acid, and therefore, 3D printed simplified the fabrication process without compromising its performance.

The reports on printed 2D material biosensors are minimal. Most of them are based on graphene-related materials and their use in detecting biomolecules or monitoring human body activities by pressure sensors. However, MXenes appear to be a promising material platform for printable and wearable sensors and pioneered by Guo et al. [98]. Guo and coworkers developed a highly sensitive, flexible, and degradable pressure sensor for the

first time to predict the health status of patients by mapping the skin (i.e., electronic skin). They explained that the flexible-pressure sensor could be attached to the human skin to obtain several biomonitoring tasks, such as measuring the physical force of the wrist, as a potential application for the healthcare prediction of early-stage Parkinson's disease. Similarly, Cheng et al. [99] fabricated a simple abrasive paper stencil printing process an MXene-based piezo-resistive sensor with randomly distributed spinous microstructures for monitor body activities and medical states by placing on joints or muscles.

In the same wearable sensors, temperature sensors are experiencing rapid growth for monitoring on-skin temperature (Figure 4), enabling real-time tracking. For the first time, Wang and coworkers fabricated a stretchable temperature sensor consisting of a cellular graphene/polydimethylsiloxane composite through a direct 3D ink-writing technique [100]. The ink was distributed into four different shapes to achieve better temperature sensitivity, a grid, triangular, and hexagonal porous structure, and the solid structure used for comparison (Figure 4a–c). The authors claimed a high-temperature sensitivity of 0.008 °C for all the printed composites. Nevertheless, the temperature sensitivity of the solid structure (i.e., rigid) decreased upon the application of external deformations. In contrast, the sensitivity of the printed grid structure showed stable results even under large external deformations (Figure 4d,e), therefore showing the high potential of flexible devices.

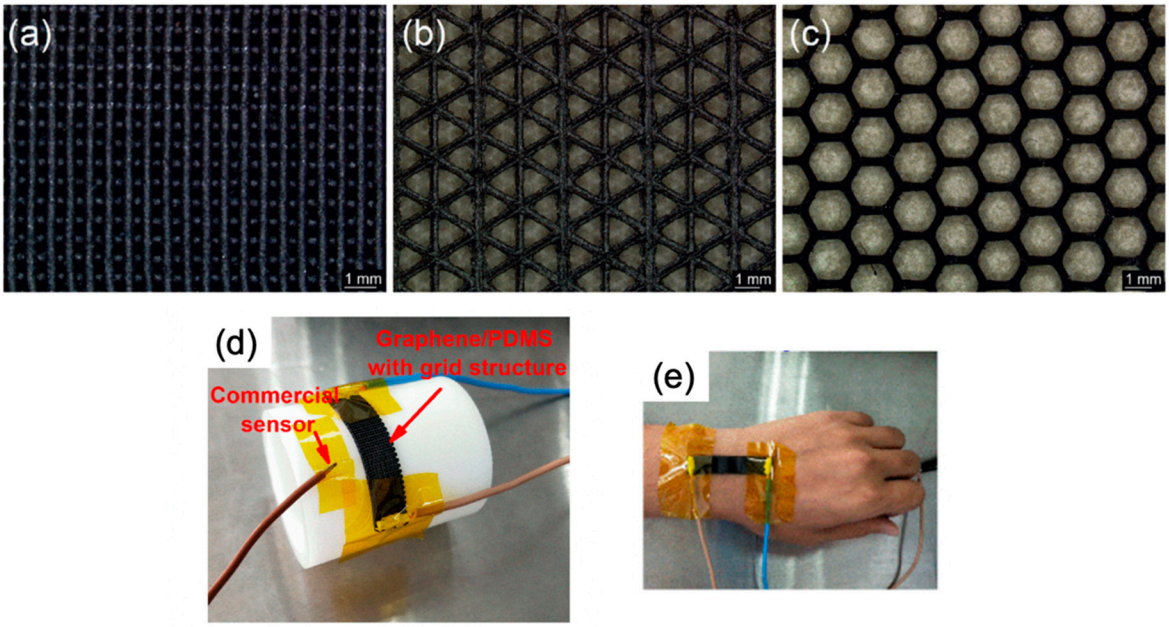

Figure 4. Optical images of the 3D-printed graphene/PDMS composites: (**a**) grid structure; (**b**) triangular porous structure; and (**c**) porous hexagonal structure. Monitoring the cooling process on a curved surface, (**d**) experimental setup, (**e**) simultaneous monitoring of wrist skin temperature. 2019, American Chemical Society©.

3.1.2. Chemical Sensors

The rapid industrial development that we are facing has led to an improvement in our daily life. Nevertheless, this fast growth has a huge environmental cost with, for instance, the emission of a series of gas pollutants such as nitrogen oxides, carbon oxides, and ammonia. In this regard, a precise determination of the toxic gas concentration might prevent us from being harmed and herein, gas sensors play a role.

Most of the reported works for gas and humidity sensing are based on graphene due to its surface area, abundant reaction sites, and superior sensing performance [101,102]. However, black phosphorus has been used to respond to humidity, showing response to H_2, O_2, and CO_2, and increased resistivity on exposure to NH_3 [103,104]. He and co-workers fabricated via inkjet-printed an ultrasensitive humidity sensor with the fast dynamic response using BP as sensing materials combined with silver nanoparticle elec-

trodes [105]. The resulting sensor showed a response time of 4.7 s and a recovery time of 3.0 s. Interestingly, the sensor also presented excellent repeatability after several cycles.

As for graphene, Kim and his group fabricated nanowires from reduced graphene oxide (rGO) without any supporting material using a nanometer-scale 3D printing approach that exploits a size-controllable liquid meniscus for freestanding writing [106]. The as-prepared rGO nanowires were used as 3D transducers in gas sensors for the detection of CO_2. Overall, the electrical conductivity of rGO was dependent on the CO_2 concentration. Thus, the electron transfer from the adsorbed CO_2 to rGO leads to increased electrical resistance. However, the sensitivity of the gas sensor was still low, and changes in the resistance were reversible at room temperature. Similarly, hollow polymer architectures based on graphene were used to detect methane, ethylene glycol, and ethanol because of interactions between molecular and defective sites on rGO sheets [107]. In detail, the complex structure ink was made from GO/ethylenediamine via hydrothermal assembly, followed by freeze-drying strategies (Figure 5). The hollow polymer architectures were based on graphene printed by a mask image-projection-based stereolithography (MIPSL).

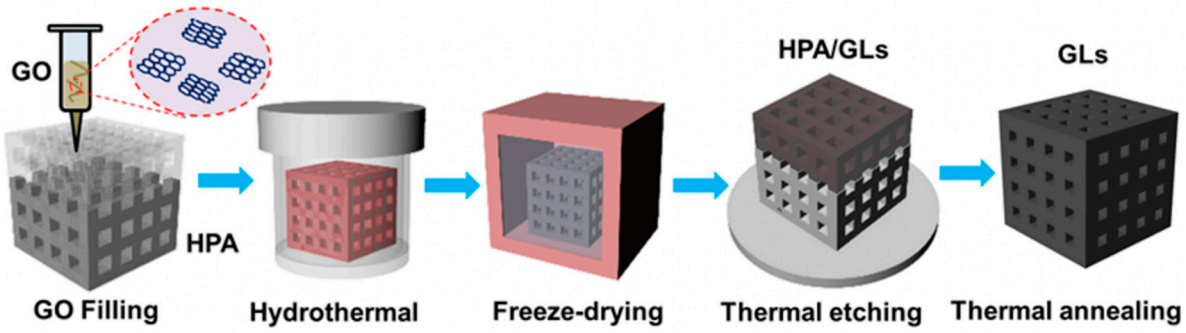

Figure 5. The schematic of 3D graphene lattices fabrication within hollow polymer architectures template ref. [78] Copyright 2018, American Chemical Society©.

MoS_2 nanosheets have been attracting interest due to their unique material properties. However, the lack of a reliable large-scale production method impedes to fulfill their potential for applications. Thus, Yao et al. [108] developed a scalable method to fabricate high concentration aqueous dispersions of MoS_2. Furthermore, they presented an inkjet printing method for large-area fabrication of MoS_2 for gas sensor devices. The MoS_2-based gas sensors demonstrated good sensitivity when exposed to NH_3, with a detection capability of several ppm of NH_3 (5 ppm).

3.1.3. Physical Sensors

Most of the physical related sensors are based on strain sensors. In detail, strain sensors, known as strain gauges, transduced tensile and pressure deformations to electrical signals. Therefore, a conductive pattern is needed, and it will be capable of producing an electrical read-out upon a deformation. Graphene has been widely used as a standard material for strain sensor fabrication combined with conductive polymers to enhance their properties. Apart from graphene, reports on 3D printed strain sensors with 2D material remain scarce.

Overall, proof-of-concept sensors based on 2D materials from graphene have been widely reported, such as sensors using inkjet-printed graphene on paper [109], by extrusion printing [110], and using extrusion inks in a cold bath (−25 °C) [78]. All of them were viable for printable 2D material sensor development due to their simple, flexible device design and easy read-out stimuli [111].

Flexible wearable strain sensors have drawn significant attention due to their broad application. However, the viscosity of the polymer composites, and the signal fluctuation caused by large deformations, especially stretching, need to be considered. Recently, the groups of Shi and Wang have commented on and address these problems [100,112,113].

For the first time, Shi and co-workers fabricated a 3D extrudable polydimethylsiloxane/graphene aqueous ink for strain sensor (Figure 6) [112]. Direct ink writing is a versatile 3D printing technique. However, the direct ink writing of conductive polymer composites is challenging due to their viscosity and most of the commercial polymer composites have a watery consistency. The inks will not hold their shape after direct ink writing extrusion. In this work, the authors overcome this challenge using ink-based polydimethylsiloxane (PDMS) sub-microbeads, electrochemically derived graphene oxide sheets (EGO), and PDMS pre-polymer. Owing to the binding effect of PDMS pre-polymer and agglomeration of PDMS sub-microbeads/EGO, the ink possessed viscoelastic behavior and maintained its structure after extrusion. The nanocomposite ink was used to print a wearable strain sensing patch. Remarkably, the scale sensors presented excellent performance over a large working range up to 40% of the strain, a gauge factor of 20.3 and fast responsivity of 83 ms.

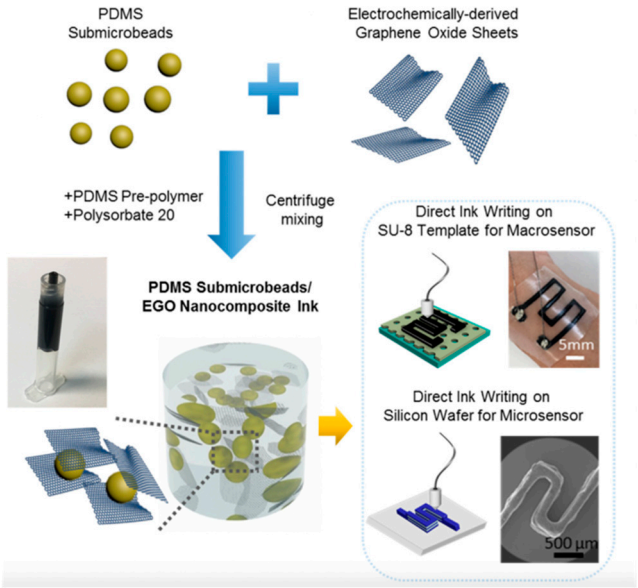

Figure 6. Schematic fabrication of PDMS sub-microbead/EGO nanocomposite ink and 3D direct ink writings wearable micro-sensor and micro-sensor. Adapted from ref. [112]. 2019, Elsevier©.

On the other hand, Wang and co-workers overcome the challenge caused by large deformations using DIW and develop various structural designs with graphene/PDMS. They elaborate and design stretchable temperature sensors [100] and strain sensors [113]. Interestingly, the use of carbon nanotubes (CNTs) could solve the great challenge of the tensile brittleness of graphene aerogels. Guo et al. [114] have reported the precisely controlled fabrication using the DIW of GO-MWCNT gel inks. The ultralight carbon aerogels were designed as strain sensors for the logic identification of sophisticated shape conversions. Notably, the resistance of the printed aerogels remained unchanged for at least 100 deformation cycles; such enhancement was ascribed to the combination of graphene sheets and MWCNTs and their cooperatively deformable 3D structures. Their methodology has opened new opportunities to highly stretchable carbon and neat inorganic materials for applications in aerospace, smart robots, and wearable devices.

3.2. Biomedical Applications

The fabrication of 3D printed constructs containing carbon-based 2D materials, transition-metal oxides, and transition-metal dichalcogenides, have emerged as new promising resources for multiple biomedical applications, in particular tissue engineering and cancer treatment [115–118]. On one side, their ability to alter the surface properties of tissue scaffolds and thus improve their biocompatibility and cell affinity make them excellent candidates in tissue engineering. On the other, their photothermal activity can be a potent tool to effectively kill cancer cells and inhibit tumor growth. In this section,

we will review the most recent advancements in the application of 2D materials in tissue engineering and other biomedical applications and discuss each one advantages.

3.2.1. Tissue Engineering

Tissue reconstruction with the efficient restoration of morphology and functionality is a critical medical challenge. Progress in 3D printing technologies offers new opportunities for precise tissular architecture reproduction, in particular bone. At the same time, biomaterials are being designed and produced to achieve the desired functional, mechanical, and supportive features and guide cell behavior in vivo. The latest progress in biomaterials research makes the family of bidimensional carbon materials in the spotlight for their excellent regeneration ability and mechanical properties.

GO, the oxidized form of graphene, is a 2D nanomaterial that has attracted substantial interest for biomedical applications because of its unique single-plane nanostructure, outstanding mechanical properties (Young's modulus >200 GPa), large surface area, and strong protein adsorption abilities [118]. However, the current graphene (G) and GO-3D fabrication technologies are still in need of optimization and simplification to ensure fine architecture and reasonable mechanical property.

Hence, to address this issue, bio-inks of graphene, GO and reduced GO have been 3D printed and reported to enhance cell adhesion and proliferation [119]. In one example, composite inks of graphene nanoflakes and hydroxyapatite microspheres have been co-3D-printed to generate hybrid complex constructs for osteogenic and neurogenic purposes. The authors demonstrated that the hybrid material supported the viability and proliferation of mesenchymal stem cells and, as well, significantly upregulates both osteogenic and neurogenic gene expression over 14 days [120]. As well, GO has been utilized as a small molecule-transport vehicle. 3D printed scaffolds containing a 10% of GO showed high chondrocyte-proliferation potential, thus suggesting potential application for cartilage matrix construction. Immuno-histochemical analyses revealed new-born and mature cartilage matrix extended along the border of the cartilage and the 3D scaffold, being thicker in the presence of the GO (see Figure 7) [121]. Similarly, bio-conjugated hydrogel nanocomposite inks based on a photo-crosslinkable alginate, bio-conjugated with both gelatine and chondroitin sulfate to mimic the cartilage extracellular matrix, and graphene oxide as nanofiller were used to fabricate 3D printed scaffolds through a micro-extrusion process. Through in vitro proliferation assay of human adipose tissue-derived mesenchymal stem cells (hADMSCs), it was demonstrated that the incorporation of graphene oxide considerably improved the biocompatibility and cell proliferation. Notably, the scaffolds produced were able to guide the cell proliferation following the direction of the 3D printed threads. In addition, the bio-conjugated alginate hydrogel matrix induced chondrogenic differentiation without exogenous pro-chondrogenesis factors as concluded from immunostaining after 28 days of culture, suggesting their potential for cartilage tissue engineering [122].

On the other side, graphene-based 3D printed scaffolds were also used for other regenerative purposes. For instance, dispersed graphene has been blended with gelatin (Gel) and sodium alginate (SA) to prepare 3D-printed scaffolds in multiple ratios. The biocompatibility tests employing PC12 neuronal cells, showed that the scaffold with Gr/Gel/SA ratio of 0.08: 6:2 was found to have better water absorption, porosity, compression modulus, hydrophilicity and cellular compatibility (proliferation and differentiation) [123]. Very recently, a GO ink was used to produce a micro-porous 3D structure by micro-extrusion-based 3D printing technology followed by an optimized freeze-drying process [124]. The resulting scaffolds showed improved rheological properties and excellent printing performance via high-speed centrifugation and ferric ion-assisted cross-linking. Additionally, cellular adhesion and viability were verified by inoculation and culture of HepaRG cells within the fabricated GO 3D structure, thus suggesting the ferric ion-assisted cross-linking and controllable pore distribution improve the performance of GO construct as a bio-scaffold also for in vitro liver tissue models [124].

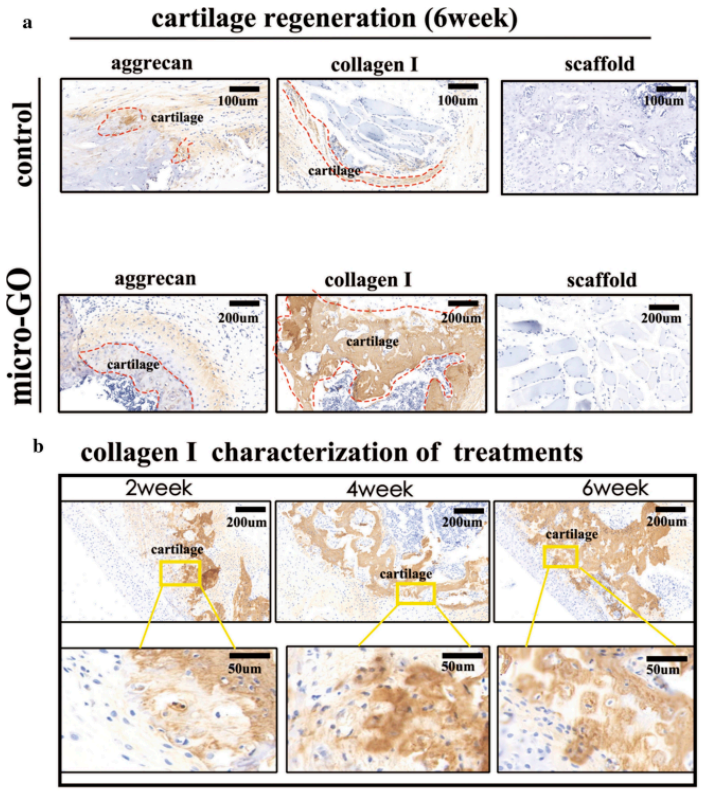

Figure 7. (**a**) Analysis of immunofluorescence staining with aggrecan and collagen I showing that the cartilage with 3D-printed scaffold only was thinner than that with micro-GO scaffold after six weeks (bar = 200 μm). (**b**) Significant differences of immunohistochemical collagen I in treatment with micro-GO scaffold from weeks 2 to 6 (bar = 200 μm, 100 μm, respectively). Adapted from ref. [121].

Boron nitride (BN) in its graphene form is an isoelectric analogue of graphite. It has been used to improve the incompatibility of multiple biodegradable synthetic materials with biological tissues [125,126]. Among the different nanofillers to reinforce polymer matrices, BN is an electrical insulator, and it has major chemical, mechanical, and thermal stability [127].

However, the literature of the developed 3D printed scaffolds containing BN is very scarce, and their main application is bone tissue engineering. For instance, PVA/hBN/bacterial cellulose (BC) 3D printed scaffolds showed a significant increase in human osteoblast cell viability for PVA/hBN/NC at a ratio of 12:0.25:0.5 [128]. It was reported BN addition improved the mechanical properties of the composites and increased the thermal stability and swelling degree of the composite hydrogels [129]. In another example, FDM based 3D printing was used to produce biomimetic biodegradable scaffolds made of PLA and exfoliated BN [130]. Apart from improving the mechanical and thermal properties of PLA, it was demonstrated that the 0.1% EBN addition favored the attachment, proliferation, and differentiation of cells with osteogenic potential and promoted the scaffold's mineralization.

3.2.2. Dual Functionality: Bone Tumor Therapy and Regeneration

The treatment of malignant bone tumors has become a significant clinical challenge due to the limited self-repair after critical damage. Current passive artificial implants must be surgically removed after recovery. Therefore, it is required an ultimate therapy that includes the removal of tumor tissues and, simultaneously, the regeneration of bone defects [131]. Bifunctional 3D scaffolds with functions in both tumor therapy and tissue engineering have been pointed as the ultimate materials to address this need [93]. To date, there are a few biomaterials possessing such dual functions, the disadvantages some of them present, however, such as long-term toxicity and degradation, restrict their application. Among the different 2D nanomaterials, particularly carbon-based 2D materials,

transition-metal oxides, and transition-metal dichalcogenides, have emerged as a new promising resource to fulfill that role, as represented in Figure 8 [115–118]. On one side, their ability to alter the surface properties of tissue scaffolds and thus improve their biocompatibility and cell affinity make them excellent candidates in tissue engineering. On the other, their photothermal activity can be a potent tool to effectively kill cancer cells and inhibit tumour growth.

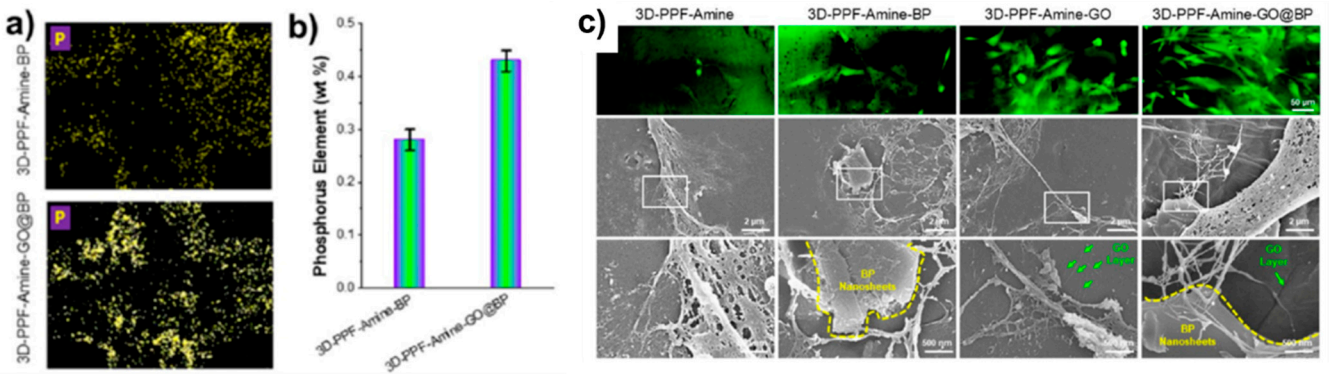

Figure 8. (**a**) Phosphorous elemental mapping on 3D scaffolds functionalized with BP and GO@BP nanosheets and (**b**) calculated amount of phosphorus content. (**c**) Immunofluorescence and SEM images showing the morphology of MC3T3 pre-osteoblast cells after 1 day of growth on functionalized 3D scaffolds (yellow lines indicate the edges of BP nanosheets; green arrows point to GO layers). Adapted with permission from ref. [118]. Copyright 2019 American Chemical Society.

In contrast to GO, BP is an under-studied 2D material with great potential in tissue engineering because of its in-plane anisotropy that originates from a unique puckered orthorhombic structure. Such configuration provides a high surface to volume ratio that can significantly increase the loading capacity [116]. The surface of BP is negatively charged due to the phosphoric acid and can thus encapsulate positively charged drug molecules or nanoparticles by electrostatic interactions within the interlayer spaces. Furthermore, BP has excellent optical properties, good biocompatibility, and biodegradability. These properties captured its attention in multiple biomedical applications, including drug delivery, bone and cancer optical therapy, wound healing, neurodegenerative treatments, biological imaging and sensing and regenerative implants [116,132–137].

Moreover, BP can degrade to produce phosphate ions or phosphonates in aqueous solution, which are required during skeleton development and bone regeneration and plays an important role in stimulating osteogenesis and osteointegration [118]. Thus, BP has been proposed as a mineral source to fabricate mineralized scaffolds for bone regeneration [137]. However, currently, the utilization of this biodegradation product for tissue engineering is still in its infancy, with limited reports on this topic. In that line, Liu et al. [118] have investigated the synergistic effect of GO and BP on cell osteogenesis for bone tissue engineering. BP was first wrapped in negatively charged GO nanosheets, which were then adsorbed together onto positively charged poly(propylene fumarate) 3D printed scaffolds. As demonstrated by the authors, the increased surface area provided by GO nanosheets enhanced cell attachment at the initial stage. In addition, slow oxidation of BP nanosheets wrapped within GO layers generated a continuous release of phosphate, which enhance the proliferation of pre-osteoblasts and also enhance scaffold mineralization and cellular differentiation, as shown in Figure 8 [118].

In another example, BP reinforced 3D-printed bio-glass scaffolds were prepared to provide a bifunctional BP-BG scaffold for photothermal therapy of osteosarcoma and in situ bone regeneration as well [138]. The in-situ phosphorus-driven, calcium-extracted biomineralization of the intra-scaffold BP nanosheets enabled both photothermal ablation of osteosarcoma and guided bone regeneration in vitro, which connects the whole therapeutic processes for better therapeutic outcome. Additionally, a corrugated structure analogous to Haversian canals was found on newborn cranial bone tissue of Sprague–Dawley rats, which

may provide much inspiration for the future research of bone-tissue engineering [138]. Finally, using the same "ablation + regeneration" concept, water/poly(lactic-co-glycolic acid)/dichloromethane emulsions containing β-tricalcium phosphate (β-TCP), 2D black phosphorus (nanosheets, low-dose doxorubicin hydrochloride (DOX) and high-dose osteogenic peptide were cryogenically 3D printed into hierarchically porous and mechanically strong nanocomposite scaffolds [139]. These scaffolds were aimed at the elimination of tumor cells with recurrence suppression and improved tissue regeneration sequentially taking advantage of the synergistic effects of photo-thermotherapy and chemotherapy. Improved bone regeneration was obtained eventually due to the presence of bony environment and sustained peptide release. Notably, BP nanosheets in scaffolds significantly reduced the long-term toxicity phenomenon of released DOX during in vivo bone regeneration [139].

The main difference between TMDCs and the other discussed 2D materials for biological applications is related to the easiness of exfoliation and possible surface modifications. As with the already discussed 2D materials, TMDCs relatively high photothermal coefficient makes them suitable for dual model cancer therapy [140]. As well, the massive surface area to volume ratio of TMDC nanosheets suggests the suitability for enhanced drug loading and targeted sustainable drug release. Bone regeneration scaffolds made of TMDCs compounds showed enhanced mechanical strength, which holds them as promising materials for tissue engineering scaffold designing and 3D printing [140]. Moreover, various imaging guided therapies are possible without invasive ionizing radiations using TMDC materials. Even though the existing vast possibilities, 3D printed TMDCs-based composites have been used as scaffolds for bone tissue engineering, targeted drug delivery and cancer therapy [140].

As with BP, TMDC bifunctional scaffolds have been developed to integrate anti-tumor/bone repairing purposes, aimed at treating the tumor and facilitating bone growth simultaneously, thus offering a promising clinical strategy to treat tumor-induced bone defects. In a first example, borosilicate bioactive glass was covered by a MoS_2-PLGA film photothermal therapy (PTT) [94]. In this study, the MoS_2-integrated composite BG (BGM) scaffolds were able to elevate temperature rapidly and effectively, exhibiting excellent photothermal stability. In addition, the BGM scaffolds were demonstrated to effectively reduce the viability of osteosarcoma cells (MNNG/HOS) in vitro and inhibit the tumor growth in nude mice. Furthermore, these BGM scaffolds were able to stimulate the proliferation and differentiation of rat bone mesenchymal stem cells (rBMSCs), upregulate the expression of osteogenesis-related genes (Runx-2, OCN and Col-I) in vitro and promote in vivo bone repair in critical-sized rat calvariae defects [94]. Wang and co-workers also fabricated bifunctional MoS_2-AKT bio-ceramic scaffolds by combining 3D printing with a hydrothermal method [93]. The inclusion of MoS_2 nanosheets endowed the bio-ceramic with photo-thermal therapeutic potential: under near-infrared (NIR) irradiation, the temperature of the MS-AKT scaffolds rapidly increased and was effectively modulated by varying the MoS_2 content, scaffold sizes and laser power densities. The photothermal temperature significantly decreased the viability of osteosarcoma cells and breast cancer cells and inhibited tumor growth in vivo. Moreover, the MS-AKT scaffolds supported the attachment, proliferation and osteogenic differentiation of bone mesenchymal stem cells and induced bone regeneration in vivo [93]. In a last example, the elements (Cu, Fe, Mn, Co)-doped bioactive glass-ceramic scaffolds were prepared via 3D-printing method [141]. Such constructs demonstrated significant photo-thermal anti-tumour effect and osteogenic differentiation ability, displaying the following trend: Cu-BG > Fe-BG > Mn-BG > Co-BG. More specifically, the hyperthermia induced by Cu-BG, Fe-BG and Mn-BG effectively killed tumour cells in vitro and inhibited tumour growth in vivo. More importantly, Fe-BG and Mn-BG scaffolds could promote rabbit bone mesenchymal stem cells adhesion, and the ionic products released from elements-doped scaffolds significantly stimulated the osteogenic differentiation of bone-forming cells. These results suggested that Fe-BG and Mn-BG scaffolds had promising potential for photothermal treatment of bone tumour and at the same time for stimulating bone regeneration [93].

Mxenes are a new class of transition metal carbides, nitrides and/or carbonitrides, which have enriched the 2D material family to interface with biological systems and serve as scaffolds in biomedical applications. In contrast to the other 2D materials discussed previously, Mxenes present unique features that make them emerge in medicine. For instance, the abundance of functional groups on the MXenes surface provides reactive sites for further functionalization with enzymes or drugs. Moreover, Mxenes present a hydrophilic surface, which makes them soluble in aqueous solutions. Finally, the high surface area and metallic conductivity are highly desirable for non-interference and low noise in biosensors, as was discussed previously.

In particular, the integration of MXene within 3D-printing BG scaffolds for achieving concurrent bone-tumor killing by photonic hyperthermia and bone-tissue regeneration was successfully achieved [142,143].

For instance, Pang and co-workers modified a 3D-BG scaffold soaking the devices in an aqueous solution of Ti_3C_2 (Figure 9) [142]. The designed device was tested in vitro and in vivo, and remarkably the dual functionality of bone-tumor killing and bone-tissue regeneration was demonstrated. The authors have demonstrated that the Ti_3C_2 accelerates the growth of newborn bone tissue of the composite BG scaffolds. Furthermore, it was observed that the scaffolds induced the death of bone cancer cells and eradicated the tumor on bone-tumor xenograft by NIR irradiation. Similarly, Ying et al. [142] used Nb_2C into 3D-BG for osteosarcoma treatment.

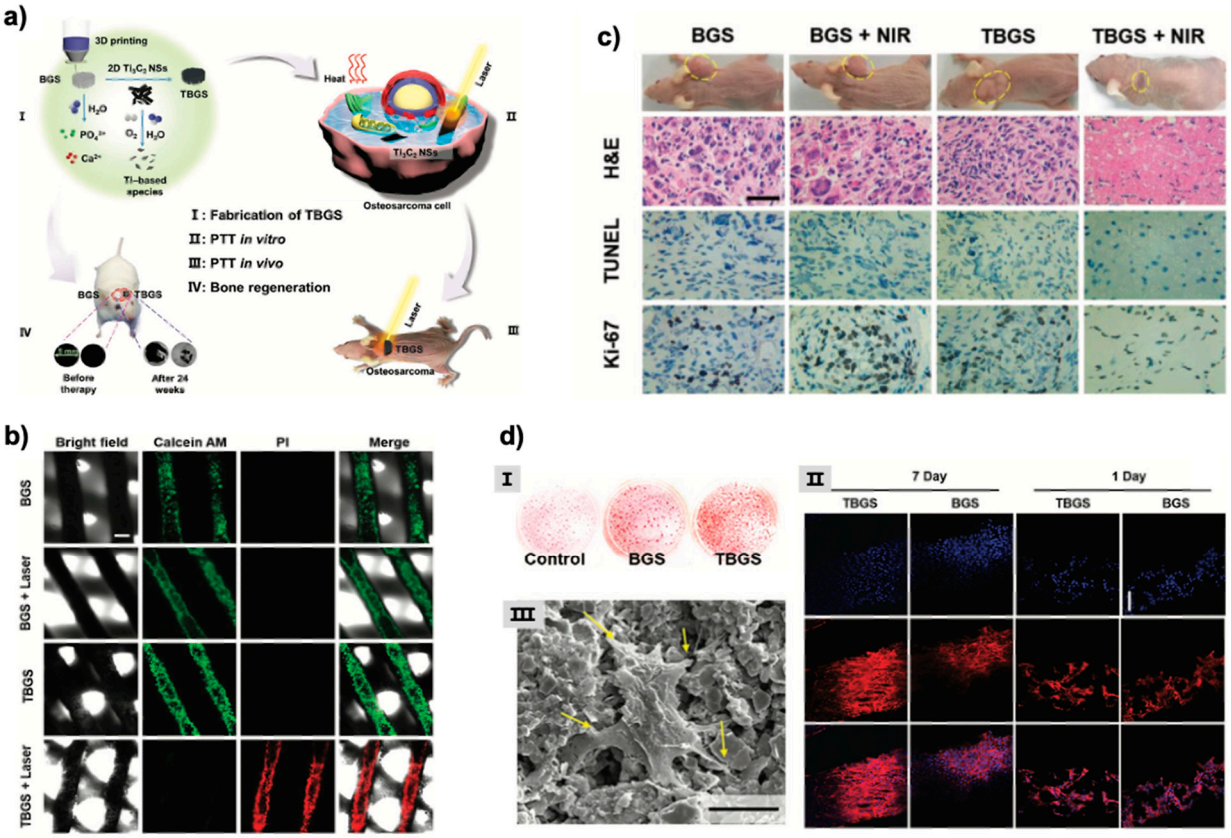

Figure 9. (**a**) Schematic illustration of the fabrication of TBGS, ablation of bone cancer, and regeneration of bone tissue: (I) Fabrication procedure of TBGS, including 3D printing of pure BGS, integration of Ti3C2 MXene, and degradation of Ti3C2 MXene on BGS. (II, III) TBGS used for osteosarcoma cell elimination by photothermal ablation both in vitro (II) and in vivo (III). (IV) Bone-tissue reconstruction and the therapeutic results after the implantation of BGS and TBGS. (**b**) In vitro photothermal-performance evaluation of TBGSs: CLSM images of live (green) and dead Saos-2 cells (red) on BGSs or TBGSs with different treatments. Scale bar is 200 mm. (**c**) In vivo photothermal-performance evaluation of TBGSs: Photographs of

Saos-2 tumor-bearing mice on 14th day after different treatments, and the tumor tissues stained by H&E, TUNEL (apoptosis), and Ki-67 (proliferation) in 1 day after different treatments (scale bars: 10 mm). (**d**) In vitro evaluation on the proliferation and osteogenic differentiation as assisted by BGS/TBGSs for bone regeneration: (I) Alizarin red S staining of control, BGSs, and TBGSs at day 21. (II) CLSM images of hBMSCs stained with DAPI (cell nuclei, blue) and rhodamine phalloidin (cytoskeleton, red) on BGSs/TBGSs at days 1 and 7 (scale bar: 100 mm). (II) SEM image of hBMSCs after seeding on 1.0 TBGS for 1 day (scale bar: 5 mm). Adapted from ref. [142].

In another example, Nb_2C modified the 3D-printed BG to effectively treat bone metastasis of breast cancer [95]. In this work, the authors have coated the surface of the MXene with a mesoporous silica layer and then the immune adjuvant (R837) was loaded into the mesopores of the composite. Finally, the composite Nb_2C@SiR NSs were integrated onto the 3D-BG scaffolds. The final biodegradable scaffold demonstrated its potential to eradicate primary tumors, activate the immune response, and suppress metastases. Remarkably, the combined therapy stimulated the host to establish a robust long-term immune memory, which provided long protection against breast cancer, including bone metastasis of breast cancer.

3.3. Energy Storage

Batteries and supercapacitors are the most common forms of energy storage devices. The traditional materials used in supercapacitors typically include carbonaceous materials, metal oxides, conductive polymers and metal organic frameworks [144–146]. Nevertheless, in this new nano era, novel 2D nanomaterials such as MXenes are paying attention. The current progress is focused on printed supercapacitors, including potential print high-speed, low-cost devices for both batteries and supercapacitors. Thus, the 3D printing of functional 2D material inks with suitable characteristics for printed batteries and energy storage devices will comment in the following section.

Several low-cost 3D printing technologies were already explored to provide unique platforms for energy storage using graphene. One of the most used protocols is based on inkjet printing. For instance, Hyun and co-workers reported a micro-supercapacitor with a planar digitated structure on a flexible plastic substrate [147]. Similarly, Lee et al. [148] fabricated a stable GO ink for inkjet printing onto Ti foils. Afterward, a thermal reduction of the printed GO was carried out to produce the electrically conductive graphene electrodes. The capacitance of the as-prepared electrodes ranged from 48 to 132 F/g, depending on the potential scan rate. Notably, the performance of the 3D printed electrodes was improved in comparison with the graphene electrodes prepared by other methods. On the other hand, screen-printed methods are well known to create graphene electrodes for supercapacitors combined with conductive polymers or plastic filaments such as PC, ABS and PLA [87,149–151].

3D printed structures from graphene aerogels were used as electrodes for supercapacitors. For instance, Li and co-workers prepared graphene aerogels via room-temperature freeze gelation [152]. Similarly, the group of Liu developed these novel aerogels creating an extrudable graphene oxide-based composite ink and modifying the 3D printing method to accommodate aerogel processing [153]. Overall, the 3D-printed graphene aerogel electrodes are lightweight, highly conductive, and exhibit excellent electrochemical properties.

In 2019, the first three-dimensional freeze printing method for MoS_2-reduced graphene oxide aerogels was reported. Brown et al. [77] manufactured a porous electrode material based on MoS_2-graphene aerogels for sodium-ion battery anodes, using a 3D freeze-printing method. They were able to control the microstructure of the hybrid materials towards the macroscopic architectures, using as an ink MoS_2 combined with a single layer of GO. Afterward, the ink was freeze-drying and thermal annealing. The result was a hybrid structure consisting of MoS_2 nanoparticles anchored on the surface of a highly porous rGO framework. The later interconnection between the MoS_2 nanoparticles and the 3D aerogels facilities improves the electrical conductivity thanks to the fast ion transport. The potential of the hybrid for electrical energy storage in sodium-ion batteries was evaluated by the authors and presented a high specific capacity changing from ~800 to

429 mAh/g at 100 mA/g, which involves both reversible 2 Na^+ insertion and irreversible conversion of MoS_2 into metallic Mo.

Inkjet printing protocols can provide an attractive route for the low-cost performance of micro-supercapacitors. Thus, continuous with inkjet printing methods, Shao and co-workers prepared an electrohydrodynamic-assisted approach (i.e., electrospray) to prepare a 1T phase dominated by 3D crumpled MoS_2 as a powder and its stable ink formation for inkjet printing for micro-supercapacitors [83]. MoS_2 is considered a promising material for energy storage. Nevertheless, due to its tendency to aggregate, their practical use was not guaranteed. Shao and colleagues have proposed a promising strategy to solve the restacking issue (Figure 10a). They claimed that the ultrathin MoS_2 sheet should be converted to 3D atomic thick building blocks without sacrificing the intrinsic atomic thickness for inkjet printing. Finally, they inkjet-printed 96 rigid asymmetric micro-supercapacitors with a high output voltage of 1.75 V in an aqueous electrolyte (Figure 10). Furthermore, the final device presented excellent capacitance retention of 96% over 20,000 cycles.

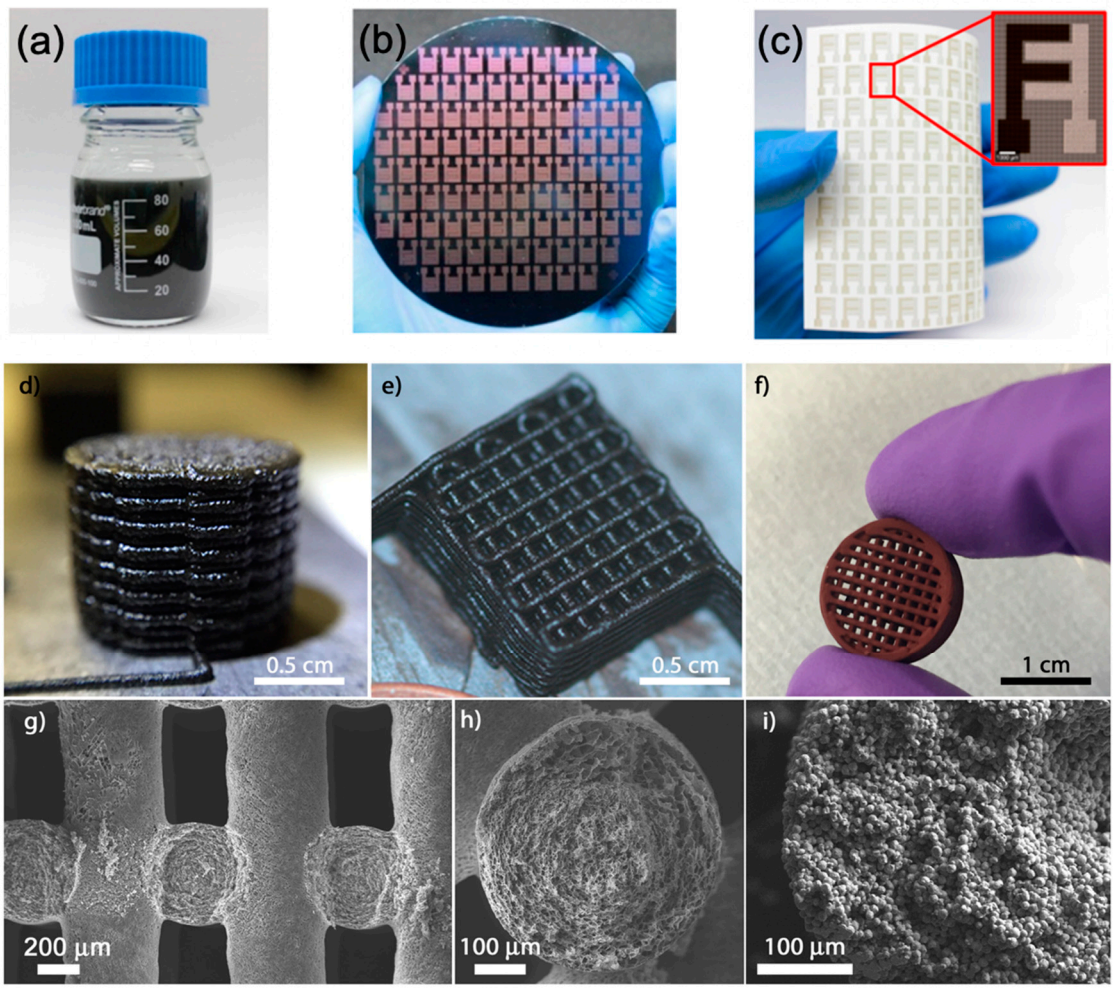

Figure 10. (**a**) c-MoS_2 ink. (**b**) 96 inkjet-printed interdigital 3D 1T c-MoS_2 MSCs on a 4 in. Si wafer. (**c**) 96 inkjet-printed 3D 1T c-MoS_2/rGO based AMSCs on flexible photopaper. Inset: Optical microscopic image of a single AMSC. Adapted from ref. [83]. (**d**–**i**) Images of the structures from Graphene-Based electrodes for electrochemical storage after 3D printing made by Rocha et al. [148] (adapted from ref. [148]).

Extrusion-based 3D printable methods have been already studied for electrochemical energy storage devices using graphene [154,155]. However, Mxenes have started to play a role in electrochemical energy storage applications. For instance, most of the micro-supercapacitors reported in the literature, which usually rely on noble metals such as gold or platinum layers as current collectors, Peng et al. [156] have used for the first

time MXenes (Ti_3C_2Tx) as the current collector and active material to print interdigitated symmetric micro-supercapacitors directly. Indeed, they demonstrated the fabrication of noble-metal-free, solid-state all-Ti_3C_2Tx MXene MSC devices with high capacitances. For instance, Areal and volumetric capacitances of 27 mF cm^{-2} and 357 F cm^{-3}, respectively, at a scan rate of 20 mV s^{-1} were achieved. The devices also demonstrated excellent cyclic stability, with 100% capacitance retention after 10,000 cycles at a scan rate of 50 mV s^{-1}. Likewise, Yang and co-workers fabricated aqueous inks of 2D (Ti_3C_2Tx) that possessed ideal viscoelastic properties for extrusion-based 3D printing of freestanding MXene, with high specific surface area architectures different sizes and shapes [157]. They further investigated the use of the inks for micro-supercapacitors. It was claimed in this work an aerial capacitance of 2.1 F cm^{-2} and a gravimetric capacitance of 242 F·g^{-1} at 0.2 A·g^{-1}, high power and energy densities and capacitance retention above 90% for 10,000 cycles.

Most of the 3D-printed electrodes used present a poor capacitive performance due to their high thermoplastic content. Redondo et al. [158] have printed by fused filament fabrication and activated for the first time nanocarbon electrodes (e.g., graphene) followed by MXene (Ti_3C_2) functionalization. The printed electrodes were tested as electrochemical capacitors and found to give superior capacitance compared to the pristine. They claimed that Ti_3C_2 improved the performance of electrochemical capacitors using 3D-printed nanocarbon electrodes due to the ability of MXene as a conductive additive to interconnect the graphene layers and to undergo diffusion-controlled redox processes alongside surface capacitive processes.

Printed electrode using direct ink writing from black phosphorous combined with polypyrrole was used for energy storage using thermo-responsive ink. Xing et al. [74] have addressed the poor dispersibility of high concentrations of black phosphorus in an aqueous solution. Remarkably, they also overcome the flow behavior and the viscoelasticity maintained a high electrochemical activity. Both challenges were solved using the Pluronic F127 hydrogel system. The printed supercapacitor electrode demonstrated a good energy storage performance with a specific capacitance of up to 417 F·g^{-1} and excellent cycling stability.

3.4. Optoelectonics and Photodetectors

Functional printable 2D materials hold great promise for developing the technologies (i.e., devices) of tomorrow. Nowadays are playing a vital role in the electronic industry due to their good processability and their tuneability to achieve the desired electrical and mechanical properties, among others. Many electronic and mechanical applications of functional printable 2D materials in this section are of considerable interest like photodetectors and optoelectronics.

Overall, the 2D materials discussed in this review present their own unique properties, as was discussed along in the introduction, which makes them useful for electronic devices [68,159,160]. The 3D printed of 2D materials structures for electronic devices are evolving towards flexible and stretchable materials. In this case, Zhang and coworkers were aware of it and printed via fused depositing modeling 3D printed flexible circuits based on graphene for further use in organic electronic fields [16]. In detail, in this work, the authors used reduced graphene oxide mixed with Polylactic acid (PLA) for the first time. They observed that r-GO presented a process of orientation during the deposition in the extrusion process, and this orientation will help improve the conductivity of the final composite. Furthermore, the composite circuits presented a strong interface bonding force with the substrate, and the filaments from the 3D printer exhibit conductivity up to 4.76 S/cm (6 wt%). Similarly, Jakus et al. [161] demonstrated a 3D printable graphene (3DG) for electronic and biomedical applications.

Apart from graphene, including its structure, MoS_2 could lead to next-generation printed devices. Seo et al. [162] reported an alternative 2D material ink based on an inkjet printable MoS_2 ink utilizing ethyl cellulose as a binder, which apports tunability in viscosity and enhanced bulk conductivity (See Figure 11). Fully inkjet-printed MoS_2-

graphene photodetectors on both rigid and flexible substrates. In detail, they further investigated the thermal annealing, which offered ultrafast photoresponse times under 150 μs, whereas photonic annealing provided a mechanically flexible device with high responsivity over 50 mA/W.

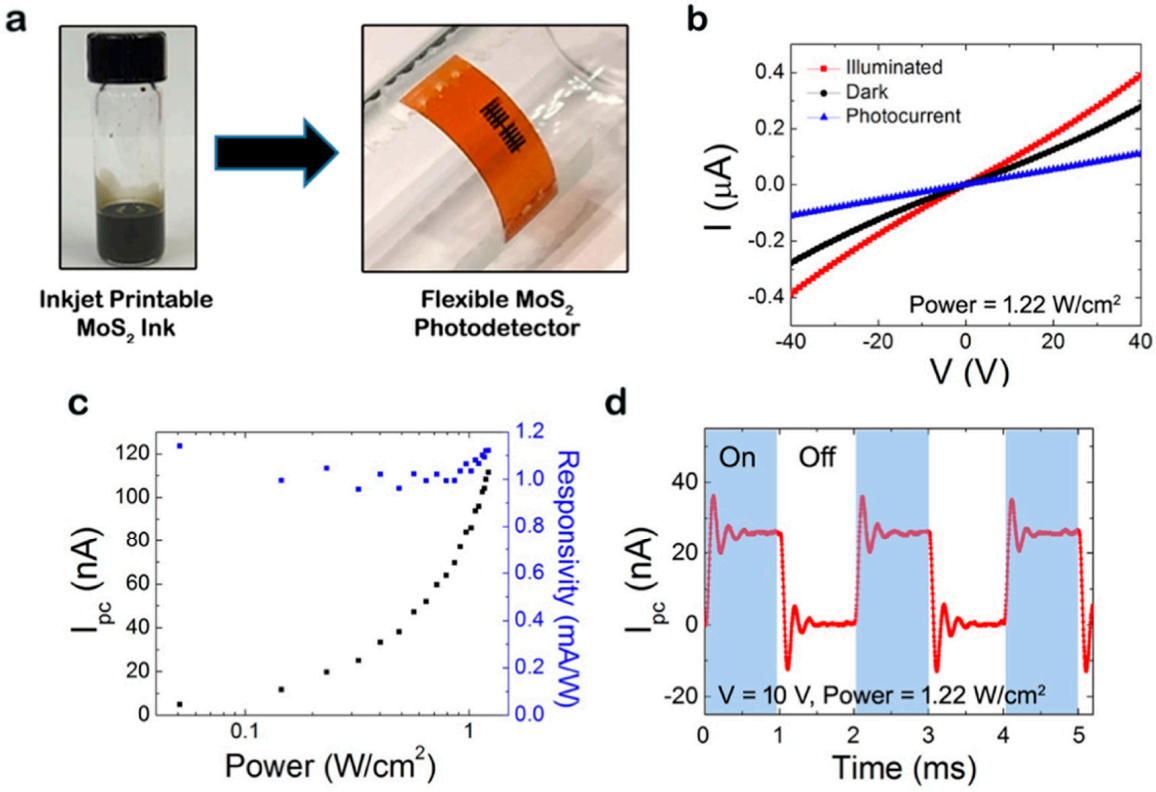

Figure 11. (**a**) Inkjet printable MoS_2 ink and its flexible photodetector. (**b**) Current-voltage curves of the MoS_2-Gr photodetector showing the dark and illuminated currents and its photocurrent. (**c**) Photocurrent and responsivity as a function of intensity at a bias. (**d**) Current modulation response at 10 V switching on and off the laser (adapted with permission from ref. [162] Copyright © 2021, American Chemical Society.

Typically, Mxenes present ultra-broadband absorption, covering the whole electromagnetic spectrum from UV-Vis, near-infrared (NIR), and THz to radio-frequency. Nevertheless, the later properties could vary depending on the composition and surface chemistry of the MXene elected. In particular, Ti_3C_2Tx is considered as the functional printable 2D material [163,164].

Wang and coworkers, for the first time, reported the fabrication of a thin-film transistors (TFTs) using spray-coating of a large-area of MXene films (Ti_3C_2) electrical contacts (i.e., including gate, source, and drain) presenting n-type (ZnO) and p-type (SnO) oxides [163]. The work function measurements of the MXene 4.60 eV (Ti_3C_2) suggested an excellent electrical contact with both oxides (ZnO and SnO), leading to good Ohmic contact formation due to the negligible band offsets between MXene and both types of semiconducting channels. In detail, the TFTs prepared displayed balanced performance, including field-effect mobilities of 2.61 and 2.01 $cm^2\ V^{-1}\ s^{-1}$ and switching ratios of 3.6×10^6 and 1.1×10^3, respectively. Furthermore, the authors investigated the complementary metal oxide semiconductor inverters and showed a large voltage gain of 80 with an excellent noise margin of 3.54 V, which is 70.8% of the ideal value. Chaudhuri et al. [165] reported that using electron beam lithography and dry etching to fabricate patterning induced Ti_3C_2Tx MXene films could increase the performance of optoelectronics. They found at NIR frequencies an intense localized surface plasmon resonance. However, further efforts still need to be addressed to obtain large-area films.

Surendran et al. [166] reported the potential application in printed electronics of hBN inks. Firstly, to this aim, the authors exfoliated hBN in DMF using a polymer-assisted liquid-phase technique. Afterward, it was adjusted the ink viscosity suitable for conventional screen printing of the ultrathin hBN nanosheets. Besides, they further studied the morphology, electrical properties, and temperature stability of the printed ink on various commercial substrates. Overall, the printed film displayed a lower dielectric constant (2.57 at 1 MHz), revealing the high potential of the prepared ink for printed electronics.

Similarly, BP could be used as photodetectors due to its moderate bandgap. Guo and coworkers explored for the first time the potential of BP thin films for photonic devices in a broad wavelength range expanding from 532 nm to 3.39 µm, the medium wavelength IR (MWIR) [167]. The prepared BP transistor exhibited an external responsivity of 82 A/W in the MWIR. Remarkably, the authors claimed that the BP transistor could detect picowatt mid-IR light even at room temperature and capability to resolve incident light polarization. These findings could help applications that require polarization sensitive light detection schemes to further enrich polarization of scattered light contains rich information about the surface roughness.

4. Conclusions and Future Perspectives

In this review, we have recapitulated the present growth and advancements of several printing techniques to form 2D material as functional inks and finally a highlight in their real-world applications such as sensors, energy storage and bio-applications (Summarized in Table 2). Despite the important number of bidimensional materials explored and reported for printing, there is plenty of room at the bottom. In the field of 3D printing of 2D materials, there is a real necessity to find elegant approaches based on chemical or physical modifications that do not only include the mixing of two components. Moreover, there is a gap in the engineering of new formulations throughout non-specific printing polymers as ionic liquids or plastic crystals.

Indeed, there are printing methodologies that have not been used for these materials, such as selective laser sintering, 2PP, and volumetric printing. These light-based printing methods are limited by high-power laser beam that selectively fuse powder printing bed, near-IR femtosecond pulse at the focal point of the laser and fast selectively binds that react in seconds, respectively. 2D materials and chemical approaches that solve the colloidal nature of the material, light-path and the intrinsic limitations of each technique are needed to overcome this lack in the literature.

Moreover, other as DLP and SLA still remain mostly unexplored for 2D materials, which means plenty of possibilities and applications in the future [69]. Besides, new approaches based on the Nanomanufacturing, which could integrate nanostructures forming devices or objects at the submicron- or nano-scale at the same time that controls shape and organization, is also of great importance [168].

The investigated applications of printable 2D material inks for smart devices have expanded various fields from electronics to biomedical. This represented the enormous potential and new opportunities of the manufactured devices. In the future, the efforts should focus on addressing the limitations of this approach and might be solved with a better combination of the 2D materials, further processing, and an optimized device design.

Table 2. Main 2D materials Printed Using Different 3D Printing Technologies and Correlation with the Electrical, Mechanical Properties, Viscosity and Final Applications.

2D Material	Shape/2D Materials	Post-Functionalized	Solvent or Plasticizer	Additives Polymers	Printing	Viscosity	Conductivity	Mech. Properties	Application	Reference
BN	Nanosheet	-	DMSO	PVA	DIW	-	0.078 W/(m·K)		Fibers for textile	[72]
BN	Nanosheets	-	-	PLA	FDM	-	-	2–2.5 GPa	Bone Tissue Engineering	[130]
BN	Hexagonal	-	Trisolvent	PLGA	DIW	30 Pa·s	2.1 W/(m·K)		Printed bioelectronics	[73]
BN	Hexagonal	-	Bacterial cellulose	PVA	DIW	50–83 mPa.s	-	0.075–0.1 MPa	Bone Tissue Engineering	[128]
BP	Nanosheets	-	PPy	PEO-PPO-PEO	DIW	-	-	-	Energy storage	[74]
BP	Nanosheets	-	-	PLGA	DIW	-	-	4–4.5 MPa	Therapy and regeneration	[138]
MoS_2	Sheet	-	PNAM	-	Screw-DIW	3.20 Pa·s	-	-	NIR activated drug Nano carriers	[76]
MoS_2	Self-assembled	-	-	PEDOT:PSS	IJP	0.2–104 Pa·s	5.2–26 S/cm	-	Super capacitors	[86]
MoS_2	Nanosheets/ Nanoflowers	Hydrothermal	-	Ceramics-Pluronic F127	DIW	-	-	-	Tissue regeneration	[93]
MoS_2	Borosilicate glass	Hydrothermal	DCM	PLGA	DIW	-	-	-	Tissue regeneration	[94]
MoS_2	MoS_2, WS_2	-	-	ABS, PETG	FDM		0.2–0.3 W/(m·K)	-	Composites	[79]
MoS_2	Graphene	Spray-coating	Commercial spray	PLA	FDM	-	-	-	Hydrogen evolution	[89]
MoS_2/rGO	Nanoflakes	-	Deionized (DI) water	-	DIW	-	-	-	3D aerogels	[77]
MoS_2/rGO	3D crumpled	-	MiliQ water:2-butanol	-	IJP	2.1 mPa·s	20.8 S/cm	-	Micro super capacitors	[83]
GO	Sheet	-	MiliQ water/DMF	PEGDA	SLA	-	64 S/m	-	3D aerogels	[80]
GO	Sheet	-	PANI Nanofibers	PEGDA	DLP	-	4.00×10^{-9} S/cm	-	3D Composites	[81]
GO	Sheet	-	Not defined	Polyurethane	DLP	-	8.05×10^{5} Ω/sq	-	3D Composites	[82]
GO	Sheet	-	Water	Biopolymer	DIW	20–50 Pa·s	-	60–100 kPa	Tissue Engineering	[122]
GO	Sheet	*MiliQ water*	-	Triton-X 100	IJP	-	15 S/cm		3D composite	[102]
GO	Sheet	-	DCM/EGO	PDMS	DIW	1.42 kPa·s	1660 Ω·cm	1242 Pa·s	Tactile sensor	[112]
GO	Sheet	-	-	Collagen-Chitosan	DIW	-	-	-	Cartilage Tissue Enginenering	[121]
rGO	Sheet	Hydrothermal	Ethylenediamine	-	-	-	0.81 S/cm	∼1.05 MPa	Sensor of Organic volatile	[107]
rGO	Nanoflakes	-	Deionized (DI) water	-	DIW	-	2.2–15.4 S/m	-	3D aerogels	[78]
rGO	Sheet	-	-	PLA	FDM	-	4.76 S/cm	-	Photodetectors	[16]

Table 2. *Cont.*

2D Material	Shape/2D Materials	Post-Functionalized	Solvent or Plasticizer	Additives Polymers	Printing	Viscosity	Conductivity	Mech. Properties	Application	Reference
Graphene	Modified graphene	-	-	Pluronic F127	DIW	10–1 × 10^5	6–13 Ω	100 kPa	3D composites	[155]
Graphene	Nanoflakes	-	Trisolvent	PLGA	DIW	30–35 Pa·s	127 S/m	3 MPa	Tissue Engineering	[120]
Graphene	-	-	-	PDMS	IJP	8–12 mPa·s	6 × 10^3 S/m	-	Micro-Supercapacitors	[147]
Graphene	GO	-	Isooctane	Silica powder	DIW	-	0.96–61.1 Ω/sq	-	Supercapacitors	[153]
Graphene	MoS_2, $MoSe_2$, WS_2 and WSe_2	Dip-coating	-	PLA	FDM	-	-	-	Hydrogen Evolution	[88]
Graphene	TMDs	Electrochemical	-	PLA	FDM	-	-	-	3D composites	[91]
Graphene	MXene	Dip-coating	-	PLA	FDM	-	-	-	Hydrogen evolution	[89]
MXene	Ti_3C_2Tx Nanoplatelets	-	-	PEG-based	IJP		1.1 × 10^4 S/m	-	Cardiac patches for tissue engineering	[86]
MXene	Nb_2C	Ball-milling	Ethyl alcohol	PVA	DIW	-	-	-	Biomedical Application	[95]
MXene	Ti_3C_2Tx Nanosheets	Screen printing	DCM	PLA	-	-	-		Wearables	[98]
MXene	Ti_3AlC_2 Nanosheets	Spray-coating	-	PDMS	IJP	-	-		Wearables	[99]
MXene	Ti_3C_2Tx Nanoplatelets	-	MiliQ/Organic solvent	-	IJP/DIW	~0.71 Pa·s	510–2770 S/m		Micro-super capacitors	[75]
MXene	Ti_3C_2Tx	MiliQ	-	-	DIW	1 × 10^3–1 × 10^4	-	-	Supercapacitors	[157]
MXene	Ti_3C_2	Electrochemical	-	PLA	FDM	-	-	36 kPa	Capacitors	[158]

Author Contributions: Conceptualization, A.D.-A. and M.V.S.; writing—review and editing, I.J.G., N.A., A.D.-A. and M.V.S. All authors have read and agreed to the published version of the manuscript.

Funding: Financial support from Operational Program Research, Development and Education-Project "MSCAfellow4@MUNI" (CZ.02.2.69/0.0/0.0/20_079/0017045) is acknowledged.

Institutional Review Board Statement: Not applicable.

Informed Consent Statement: Not applicable.

Data Availability Statement: Not applicable.

Conflicts of Interest: The authors declare no conflict of interest.

Abbreviations

2PP	Two-photon polymerization printing
3D	Three-dimensional
ABS	Acrylonitrile butadiene co-polymers
AM	Additive manufacturing
BC	Bacterial cellulose
BG	Borosilicate bioactive glass
BN	Boron nitride
BNNSs	Boron nitride nanosheets
BP	Black Phosphorous
CNTs	Carbon nanotubes
CVD	Chemical vapor deposition
DBP	Di-butyl phthalate
DCM	Dichloromethane
DIW	Direct ink writing
DLP	Digital light printing
DOX	Doxorubicin hydrochloride
EGBE	Ethylene glycol monobutyl ether
EGO	Electrochemically derived graphene oxide sheets
FDM	Fused deposition modeling
G	Graphene
Gel	Gelatin
GO	Graphene oxide
h-BN	Hexagonal boron nitride
hADMSCs	Human adipose tissue-derived mesenchymal stem cells
IKP	Inkjet printing
LPE	Liquid phase exfoliation
MIPSL	Mask image-projection-based stereolithography
NIR	Near-infrared
NMP	N-Methyl-2-Pyrrolidone
PANI	Polyaniline
PC	Polycarbonate
PDMS	Polydimethylsiloxane
PETG	Polyethylene terephthalate glycol
PLA	Polylactic acid
PLGA	Polylactide-co-glycolide
PNAM	Poly(N-isopropylacrylamide-co-acrylamide-co-2-mercaptoethylacrylamide)
PPSF	Polyphenylsulphone
PPy	Poly pyrrole
PTT	Photothermal therapy
PVA	Poly vinyl alcohol
rBMSCs	Rat bone mesenchymal stem cells
rGO	Reduced Graphene Oxide
SA	Sodium alginate
SLA	Stereolithography
TMDs	Transition metal dichalcogenides
TPU	Thermoplastic polyurethane

References

1. Ferrari, A.C.; Meyer, J.C.; Scardaci, V.; Casiraghi, C.; Lazzeri, M.; Mauri, F.; Piscanec, S.; Jiang, D.; Novoselov, K.S.; Roth, S.; et al. Raman Spectrum of Graphene and Graphene Layers. *Phys. Rev. Lett.* **2006**, *97*, 187401. [CrossRef]
2. Naumis, G.G.; Barraza-Lopez, S.; Oliva-Leyva, M.; Terrones, H. Electronic and optical properties of strained graphene and other strained 2D materials: A review. *Rep. Prog. Phys.* **2017**, *80*, 096501. [CrossRef]
3. Huo, C.; Yan, Z.; Song, X.; Zeng, H. 2D materials via liquid exfoliation: A review on fabrication and applications. *Sci. Bull.* **2015**, *60*, 1994–2008. [CrossRef]
4. Mas-Ballesté, R.; Gómez-Navarro, C.; Gómez-Herrero, J.; Zamora, F. 2D materials: To graphene and beyond. *Nanoscale* **2011**, *3*, 20–30. [CrossRef]
5. Glavin, N.R.; Rao, R.; Varshney, V.; Bianco, E.; Apte, A.; Roy, A.; Ringe, E.; Ajayan, P.M. Emerging Applications of Elemental 2D Materials. *Adv. Mater.* **2020**, *32*, 1904302. [CrossRef]
6. Iqbal, A.; Sambyal, P.; Koo, C.M. 2D MXenes for Electromagnetic Shielding: A Review. *Adv. Funct. Mater.* **2020**, *30*, 2000883. [CrossRef]
7. Tahir, M.B.; Fatima, N.; Fatima, U.; Sagir, M. A review on the 2D black phosphorus materials for energy applications. *Inorg. Chem. Commun.* **2021**, *124*, 108242. [CrossRef]
8. Chhowalla, M.; Liu, Z.; Zhang, H. Two-dimensional transition metal dichalcogenide (TMD) nanosheets. *Chem. Soc. Rev.* **2015**, *44*, 2584–2586. [CrossRef]
9. Bie, C.; Cheng, B.; Fan, J.; Ho, W.; Yu, J. Enhanced solar-to-chemical energy conversion of graphitic carbon nitride by two-dimensional cocatalysts. *EnergyChem* **2021**, *3*, 100051. [CrossRef]
10. Zhang, C.; Tan, J.; Pan, Y.; Cai, X.; Zou, X.; Cheng, H.-M.; Liu, B. Mass production of 2D materials by intermediate-assisted grinding exfoliation. *Natl. Sci. Rev.* **2019**, *7*, 324–332. [CrossRef]
11. Yao, J.D.; Zheng, Z.Q.; Yang, G.W. Production of large-area 2D materials for high-performance photodetectors by pulsed-laser deposition. *Prog. Mater. Sci.* **2019**, *106*, 100573. [CrossRef]
12. Yang, S.; Zhang, P.; Nia, A.S.; Feng, X. Emerging 2D Materials Produced via Electrochemistry. *Adv. Mater.* **2020**, *32*, 1907857. [CrossRef]
13. Chacham, H.; Santos, J.C.C.; Pacheco, F.G.; Silva, D.L.; Martins, R.M.; Del'Boccio, J.P.; Soares, E.M.; Altoé, R.; Furtado, C.A.; Plentz, F.; et al. Controlling the Morphology of Nanoflakes Obtained by Liquid-Phase Exfoliation: Implications for the Mass Production of 2D Materials. *ACS Appl. Nano Mater.* **2020**, *3*, 12095–12105. [CrossRef]
14. Park, S.; Ruoff, R.S. Chemical methods for the production of graphenes. *Nat. Nanotechnol.* **2009**, *4*, 217–224. [CrossRef]
15. Hernandez, Y.; Nicolosi, V.; Lotya, M.; Blighe, F.M.; Sun, Z.; De, S.; McGovern, I.T.; Holland, B.; Byrne, M.; Gun'Ko, Y.K.; et al. High-yield production of graphene by liquid-phase exfoliation of graphite. *Nat. Nanotechnol.* **2008**, *3*, 563–568. [CrossRef]
16. Zhang, D.; Chi, B.; Li, B.; Gao, Z.; Du, Y.; Guo, J.; Wei, J. Fabrication of highly conductive graphene flexible circuits by 3D printing. *Synth. Met.* **2016**, *217*, 79–86. [CrossRef]
17. Ye, J.; Craciun, M.F.; Koshino, M.; Russo, S.; Inoue, S.; Yuan, H.; Shimotani, H.; Morpurgo, A.F.; Iwasa, Y. Accessing the transport properties of graphene and its multilayers at high carrier density. *Proc. Natl. Acad. Sci. USA* **2011**, *108*, 13002–13006. [CrossRef]
18. Lee, G.-H.; Cooper, R.C.; An, S.J.; Lee, S.; Zande, A.V.D.; Petrone, N.; Hammerberg, A.G.; Lee, C.; Crawford, B.; Oliver, W.; et al. High-Strength Chemical-Vapor–Deposited Graphene and Grain Boundaries. *Science* **2013**, *340*, 1073–1076. [CrossRef]
19. Gómez, I.J.; Vázquez Sulleiro, M.; Mantione, D.; Alegret, N. Carbon Nanomaterials Embedded in Conductive Polymers: A State of the Art. *Polymers* **2021**, *13*, 745. [CrossRef]
20. Vázquez Sulleiro, M.; Quiroga, S.; Peña, D.; Pérez, D.; Guitián, E.; Criado, A.; Prato, M. Microwave-induced covalent functionalization of few-layer graphene with arynes under solvent-free conditions. *Chem. Commun.* **2018**, *54*, 2086–2089. [CrossRef]
21. Nine, M.J.; Cole, M.A.; Tran, D.N.H.; Losic, D. Graphene: A multipurpose material for protective coatings. *J. Mater. Chem. A* **2015**, *3*, 12580–12602. [CrossRef]
22. Novoselov, K.S.; Fal'ko, V.I.; Colombo, L.; Gellert, P.R.; Schwab, M.G.; Kim, K. A roadmap for graphene. *Nature* **2012**, *490*, 192–200. [CrossRef]
23. Nicolosi, V.; Chhowalla, M.; Kanatzidis, M.G.; Strano, M.S.; Coleman, J.N. Liquid Exfoliation of Layered Materials. *Science* **2013**, *340*, 1226419. [CrossRef]
24. Sarno, M.; Scarpa, D.; Senatore, A.; Ahmed Abdalglil Mustafa, W. rGO/GO Nanosheets in Tribology: From the State of the Art to the Future Prospective. *Lubricants* **2020**, *8*, 31. [CrossRef]
25. Agarwal, V.; Zetterlund, P.B. Strategies for reduction of graphene oxide—A comprehensive review. *Chem. Eng. J.* **2021**, *405*, 127018. [CrossRef]
26. Nurunnabi, M.; Parvez, K.; Nafiujjaman, M.; Revuri, V.; Khan, H.A.; Feng, X.; Lee, Y.-K. Bioapplication of graphene oxide derivatives: Drug/gene delivery, imaging, polymeric modification, toxicology, therapeutics and challenges. *RSC Adv.* **2015**, *5*, 42141–42161. [CrossRef]
27. Guex, L.G.; Sacchi, B.; Peuvot, K.F.; Andersson, R.L.; Pourrahimi, A.M.; Ström, V.; Farris, S.; Olsson, R.T. Experimental review: Chemical reduction of graphene oxide (GO) to reduced graphene oxide (rGO) by aqueous chemistry. *Nanoscale* **2017**, *9*, 9562–9571. [CrossRef]
28. Voiry, D.; Mohite, A.; Chhowalla, M. Phase engineering of transition metal dichalcogenides. *Chem. Soc. Rev.* **2015**, *44*, 2702–2712. [CrossRef]
29. Chaves, A.; Azadani, J.G.; Alsalman, H.; da Costa, D.R.; Frisenda, R.; Chaves, A.J.; Song, S.H.; Kim, Y.D.; He, D.; Zhou, J.; et al. Bandgap engineering of two-dimensional semiconductor materials. *NPJ 2D Mater. Appl.* **2020**, *4*, 29. [CrossRef]
30. Krishnan, U.; Kaur, M.; Singh, K.; Kumar, M.; Kumar, A. A synoptic review of MoS_2: Synthesis to applications. *Superlattices Microstruct.* **2019**, *128*, 274–297. [CrossRef]

31. Eda, G.; Yamaguchi, H.; Voiry, D.; Fujita, T.; Chen, M.; Chhowalla, M. Photoluminescence from chemically exfoliated MoS_2. *Nano Lett.* **2011**, *11*, 5111–5116. [CrossRef]
32. Jawaid, A.; Nepal, D.; Park, K.; Jespersen, M.; Qualley, A.; Mirau, P.; Drummy, L.F.; Vaia, R.A. Mechanism for liquid phase exfoliation of MoS_2. *Chem. Mater.* **2015**, *28*, 337–348. [CrossRef]
33. Coleman, J.N.; Lotya, M.; O'Neill, A.; Bergin, S.D.; King, P.J.; Khan, U.; Young, K.; Gaucher, A.; De, S.; Smith, R.J. Two-dimensional nanosheets produced by liquid exfoliation of layered materials. *Science* **2011**, *331*, 568–571. [CrossRef]
34. Sun, J.; Li, X.; Guo, W.; Zhao, M.; Fan, X.; Dong, Y.; Xu, C.; Deng, J.; Fu, Y. Synthesis Methods of Two-Dimensional MoS_2: A Brief Review. *Crystals* **2017**, *7*, 198. [CrossRef]
35. Naguib, M.; Kurtoglu, M.; Presser, V.; Lu, J.; Niu, J.; Heon, M.; Hultman, L.; Gogotsi, Y.; Barsoum, M.W. Two-Dimensional Nanocrystals Produced by Exfoliation of Ti_3AlC_2. *Adv. Mater.* **2011**, *23*, 4248–4253. [CrossRef]
36. VahidMohammadi, A.; Rosen, J.; Gogotsi, Y. The world of two-dimensional carbides and nitrides (MXenes). *Science* **2021**, *372*, eabf1581. [CrossRef]
37. Jiang, Q.; Lei, Y.; Liang, H.; Xi, K.; Xia, C.; Alshareef, H.N. Review of MXene electrochemical microsupercapacitors. *Energy Storage Mater.* **2020**, *27*, 78–95. [CrossRef]
38. Zhang, C.; Nicolosi, V. Graphene and MXene-based transparent conductive electrodes and supercapacitors. *Energy Storage Mater.* **2019**, *16*, 102–125. [CrossRef]
39. Hart, J.L.; Hantanasirisakul, K.; Lang, A.C.; Anasori, B.; Pinto, D.; Pivak, Y.; van Omme, J.T.; May, S.J.; Gogotsi, Y.; Taheri, M.L. Control of MXenes' electronic properties through termination and intercalation. *Nat. Commun.* **2019**, *10*, 522. [CrossRef]
40. Anasori, B.; Lukatskaya, M.R.; Gogotsi, Y. 2D metal carbides and nitrides (MXenes) for energy storage. *Nat. Rev. Mater.* **2017**, *2*, 16098. [CrossRef]
41. Bai, Y.; Liu, C.; Chen, T.; Li, W.; Zheng, S.; Pi, Y.; Luo, Y.; Pang, H. MXene-Copper/Cobalt Hybrids via Lewis Acidic Molten Salts Etching for High Performance Symmetric Supercapacitors. *Angew. Chem. Int. Ed.* **2021**. [CrossRef]
42. Huang, K.; Li, Z.; Lin, J.; Han, G.; Huang, P. Two-dimensional transition metal carbides and nitrides (MXenes) for biomedical applications. *Chem. Soc. Rev.* **2018**, *47*, 5109–5124. [CrossRef]
43. Guo, Z.; Zhou, J.; Zhu, L.; Sun, Z. MXene: A promising photocatalyst for water splitting. *J. Mater. Chem. A* **2016**, *4*, 11446–11452. [CrossRef]
44. Jun, B.-M.; Kim, S.; Heo, J.; Park, C.M.; Her, N.; Jang, M.; Huang, Y.; Han, J.; Yoon, Y. Review of MXenes as new nanomaterials for energy storage/delivery and selected environmental applications. *Nano Res.* **2019**, *12*, 471–487. [CrossRef]
45. Khazaei, M.; Mishra, A.; Venkataramanan, N.S.; Singh, A.K.; Yunoki, S. Recent advances in MXenes: From fundamentals to applications. *Curr. Opin. Solid State Mater. Sci.* **2019**, *23*, 164–178. [CrossRef]
46. Sajid, M. MXenes: Are they emerging materials for analytical chemistry applications?—A review. *Anal. Chim. Acta* **2021**, *1143*, 267–280. [CrossRef]
47. Verger, L.; Natu, V.; Carey, M.; Barsoum, M.W. MXenes: An Introduction of Their Synthesis, Select Properties, and Applications. *Trends Chem.* **2019**, *1*, 656–669. [CrossRef]
48. Gusmão, R.; Sofer, Z.; Pumera, M. Black Phosphorus Rediscovered: From Bulk Material to Monolayers. *Angew. Chem. Int. Ed.* **2017**, *56*, 8052–8072. [CrossRef]
49. Ren, X.; Lian, P.; Xie, D.; Yang, Y.; Mei, Y.; Huang, X.; Wang, Z.; Yin, X. Properties, preparation and application of black phosphorus/phosphorene for energy storage: A review. *J. Mater. Sci.* **2017**, *52*, 10364–10386. [CrossRef]
50. Shen, Z.-K.; Yuan, Y.-J.; Pei, L.; Yu, Z.-T.; Zou, Z. Black phosphorus photocatalysts for photocatalytic H_2 generation: A review. *Chem. Eng. J.* **2020**, *386*, 123997. [CrossRef]
51. Lee, T.H.; Kim, S.Y.; Jang, H.W. Black Phosphorus: Critical Review and Potential for Water Splitting Photocatalyst. *Nanomaterials* **2016**, *6*, 194. [CrossRef]
52. Luo, M.; Fan, T.; Zhou, Y.; Zhang, H.; Mei, L. 2D Black Phosphorus–Based Biomedical Applications. *Adv. Funct. Mater.* **2019**, *29*, 1808306. [CrossRef]
53. Li, Q.; Wu, J.-T.; Liu, Y.; Qi, X.-M.; Jin, H.-G.; Yang, C.; Liu, J.; Li, G.-L.; He, Q.-G. Recent advances in black phosphorus-based electrochemical sensors: A review. *Anal. Chim. Acta* **2021**, *1170*, 338480. [CrossRef]
54. Ferrara, C.; Vigo, E.; Albini, B.; Galinetto, P.; Milanese, C.; Tealdi, C.; Quartarone, E.; Passerini, S.; Mustarelli, P. Efficiency and Quality Issues in the Production of Black Phosphorus by Mechanochemical Synthesis: A Multi-Technique Approach. *ACS Appl. Energy Mater.* **2019**, *2*, 2794–2802. [CrossRef]
55. Antonatos, N.; Bouša, D.; Kovalska, E.; Sedmidubský, D.; Růžička, K.; Vrbka, P.; Veselý, M.; Hejtmánek, J.; Sofer, Z. Large-Scale Production of Nanocrystalline Black Phosphorus Ceramics. *ACS Appl. Mater. Interfaces* **2020**, *12*, 7381–7391. [CrossRef]
56. Brent, J.R.; Savjani, N.; Lewis, E.A.; Haigh, S.J.; Lewis, D.J.; O'Brien, P. Production of few-layer phosphorene by liquid exfoliation of black phosphorus. *Chem. Commun.* **2014**, *50*, 13338–13341. [CrossRef]
57. Zhi, C.; Ueda, S.; Zeng, H.; Wang, X.; Tian, W.; Wang, X.; Bando, Y.; Golberg, D. Weak morphology dependent valence band structure of boron nitride. *J. Appl. Phys.* **2013**, *114*, 054306. [CrossRef]
58. Liu, L.; Feng, Y.P.; Shen, Z.X. Structural and electronic properties of h-BN. *Phys. Rev. B* **2003**, *68*, 104102. [CrossRef]
59. Jiang, X.-F.; Weng, Q.; Wang, X.-B.; Li, X.; Zhang, J.; Golberg, D.; Bando, Y. Recent Progress on Fabrications and Applications of Boron Nitride Nanomaterials: A Review. *J. Mater. Sci. Technol.* **2015**, *31*, 589–598. [CrossRef]
60. Dean, C.R.; Young, A.F.; Meric, I.; Lee, C.; Wang, L.; Sorgenfrei, S.; Watanabe, K.; Taniguchi, T.; Kim, P.; Shepard, K.L.; et al. Boron nitride substrates for high-quality graphene electronics. *Nat. Nanotechnol.* **2010**, *5*, 722–726. [CrossRef]

61. Zhi, C.; Bando, Y.; Tang, C.; Kuwahara, H.; Golberg, D. Large-Scale Fabrication of Boron Nitride Nanosheets and Their Utilization in Polymeric Composites with Improved Thermal and Mechanical Properties. *Adv. Mater.* **2009**, *21*, 2889–2893. [CrossRef]
62. Cui, Z.; Oyer, A.J.; Glover, A.J.; Schniepp, H.C.; Adamson, D.H. Large Scale Thermal Exfoliation and Functionalization of Boron Nitride. *Small* **2014**, *10*, 2352–2355. [CrossRef]
63. Han, W.-Q.; Wu, L.; Zhu, Y.; Watanabe, K.; Taniguchi, T. Structure of chemically derived mono- and few-atomic-layer boron nitride sheets. *Appl. Phys. Lett.* **2008**, *93*, 223103. [CrossRef]
64. Warner, J.H.; Rümmeli, M.H.; Bachmatiuk, A.; Büchner, B. Atomic Resolution Imaging and Topography of Boron Nitride Sheets Produced by Chemical Exfoliation. *ACS Nano* **2010**, *4*, 1299–1304. [CrossRef]
65. Elder, B.; Neupane, R.; Tokita, E.; Ghosh, U.; Hales, S.; Kong, Y.L. Nanomaterial Patterning in 3D Printing. *Adv. Mater.* **2020**, *32*, e1907142. [CrossRef]
66. Chakraborty, P.K.; Azadmanjiri, J.; Pavithra, C.L.P.; Wang, X.; Masood, S.H.; Dey, S.R.; Wang, J. Advancements in Therapeutics via 3D Printed Multifunctional Architectures from Dispersed 2D Nanomaterial Inks. *Small* **2020**, *16*, e2004900. [CrossRef]
67. Lee, M.; Rizzo, R.; Surman, F.; Zenobi-Wong, M. Guiding Lights: Tissue Bioprinting Using Photoactivated Materials. *Chem. Rev.* **2020**, *120*, 10950–11027. [CrossRef]
68. Hassan, K.; Nine, M.J.; Tung, T.T.; Stanley, N.; Yap, P.L.; Rastin, H.; Yu, L.; Losic, D. Functional inks and extrusion-based 3D printing of 2D materials: A review of current research and applications. *Nanoscale* **2020**, *12*, 19007–19042. [CrossRef]
69. Criado-Gonzalez, M.; Dominguez-Alfaro, A.; Lopez-Larrea, N.; Alegret, N.; Mecerreyes, D. Additive Manufacturing of Conducting Polymers: Recent Advances, Challenges, and Opportunities. *ACS Appl. Polym. Mater.* **2021**, *3*, 2865–2883. [CrossRef]
70. Wu, R.; Zhang, H.; Pan, J.; Zhu, H.; Ma, Y.; Cui, W.; Santos, H.A.; Pan, G. Spatio-Design of Multidimensional Prickly Zn-Doped CuO Nanoparticle for Efficient Bacterial Killing. *Adv. Mater. Interfaces* **2016**, *3*, 1600472. [CrossRef]
71. Cheng, M.; Deivanayagam, R.; Shahbazian-Yassar, R. 3D Printing of Electrochemical Energy Storage Devices: A Review of Printing Techniques and Electrode/Electrolyte Architectures. *Batter. Supercaps* **2020**, *3*, 130–146. [CrossRef]
72. Gao, T.; Yang, Z.; Chen, C.; Li, Y.; Fu, K.; Dai, J.; Hitz, E.M.; Xie, H.; Liu, B.; Song, J.; et al. Three-Dimensional Printed Thermal Regulation Textiles. *ACS Nano* **2017**, *11*, 11513–11520. [CrossRef]
73. Guiney, L.M.; Mansukhani, N.D.; Jakus, A.E.; Wallace, S.G.; Shah, R.N.; Hersam, M.C. Three-Dimensional Printing of Cytocompatible, Thermally Conductive Hexagonal Boron Nitride Nanocomposites. *Nano Lett.* **2018**, *18*, 3488–3493. [CrossRef]
74. Xing, R.; Xia, Y.; Huang, R.; Qi, W.; Su, R.; He, Z. Three-dimensional printing of black phosphorous/polypyrrole electrode for energy storage using thermoresponsive ink. *Chem. Commun.* **2020**, *56*, 3115–3118. [CrossRef]
75. Zhang, C.J.; McKeon, L.; Kremer, M.P.; Park, S.H.; Ronan, O.; Seral-Ascaso, A.; Barwich, S.; Coileain, C.O.; McEvoy, N.; Nerl, H.C.; et al. Additive-free MXene inks and direct printing of micro-supercapacitors. *Nat. Commun.* **2019**, *10*, 1795. [CrossRef]
76. Lee, H.P.; Lokhande, G.; Singh, K.A.; Jaiswal, M.K.; Rajput, S.; Gaharwar, A.K. Light-Triggered In Situ Gelation of Hydrogels using 2D Molybdenum Disulfide (MoS_2) Nanoassemblies as Crosslink Epicenter. *Adv. Mater.* **2021**, *33*, e2101238. [CrossRef]
77. Brown, E.; Yan, P.; Tekik, H.; Elangovan, A.; Wang, J.; Lin, D.; Li, J. 3D printing of hybrid MoS_2-graphene aerogels as highly porous electrode materials for sodium ion battery anodes. *Mater. Des.* **2019**, *170*, 107689. [CrossRef]
78. Zhang, Q.; Zhang, F.; Medarametla, S.P.; Li, H.; Zhou, C.; Lin, D. 3D Printing of Graphene Aerogels. *Small* **2016**, *12*, 1702–1708. [CrossRef]
79. Kaul, A.B. Two-dimensional layered materials: Structure, properties, and prospects for device applications. *J. Mater. Res.* **2014**, *29*, 348–361. [CrossRef]
80. Hensleigh, R.M.; Cui, H.; Oakdale, J.S.; Ye, J.C.; Campbell, P.G.; Duoss, E.B.; Spadaccini, C.M.; Zheng, X.; Worsley, M.A. Additive manufacturing of complex micro-architected graphene aerogels. *Mater. Horiz.* **2018**, *5*, 1035–1041. [CrossRef]
81. Han, H.; Cho, S. Fabrication of Conducting Polyacrylate Resin Solution with Polyaniline Nanofiber and Graphene for Conductive 3D Printing Application. *Polymers* **2018**, *10*, 1003. [CrossRef] [PubMed]
82. Joo, H.; Cho, S. Comparative Studies on Polyurethane Composites Filled with Polyaniline and Graphene for DLP-Type 3D Printing. *Polymers* **2020**, *12*, 67. [CrossRef]
83. Shao, Y.; Fu, J.H.; Cao, Z.; Song, K.; Sun, R.; Wan, Y.; Shamim, A.; Cavallo, L.; Han, Y.; Kaner, R.B.; et al. 3D Crumpled Ultrathin 1T MoS_2 for Inkjet Printing of Mg-Ion Asymmetric Micro-supercapacitors. *ACS Nano* **2020**, *14*, 7308–7318. [CrossRef] [PubMed]
84. Silvestri, A.; Criado, A.; Poletti, F.; Wang, F.; Fanjul-Bolado, P.; González-García, M.B.; García-Astrain, C.; Liz-Marzán, L.M.; Feng, X.; Zanardi, C.; et al. Bioresponsive, Electroactive, and Inkjet-Printable Graphene-Based Inks. *Adv. Funct. Mater.* **2021**, 2105028. [CrossRef]
85. Chao, Y.; Ge, Y.; Chen, Z.; Cui, X.; Zhao, C.; Wang, C.; Wallace, G.G. One-Pot Hydrothermal Synthesis of Solution-Processable MoS_2/PEDOT:PSS Composites for High-Performance Supercapacitors. *ACS Appl. Mat. Inter.* **2021**, *13*, 7285–7296. [CrossRef]
86. Basara, G.; Saeidi-Javash, M.; Ren, X.; Bahcecioglu, G.; Wyatt, B.C.; Anasori, B.; Zhang, Y.; Zorlutuna, P. Electrically conductive 3D printed Ti_3C_2Tx MXene-PEG composite constructs for cardiac tissue engineering. *Acta Biomater.* **2020**, in press. [CrossRef]
87. Foster, C.W.; Down, M.P.; Zhang, Y.; Ji, X.; Rowley-Neale, S.J.; Smith, G.C.; Kelly, P.J.; Banks, C.E. 3D Printed Graphene Based Energy Storage Devices. *Sci. Rep.* **2017**, *7*, 42233. [CrossRef]
88. Akshay Kumar, K.P.; Ghosh, K.; Alduhaish, O.; Pumera, M. Dip-coating of MXene and transition metal dichalcogenides on 3D-printed nanocarbon electrodes for the hydrogen evolution reaction. *Electrochem. Commun.* **2021**, *122*, 106890. [CrossRef]
89. Gusmao, R.; Sofer, Z.; Marvan, P.; Pumera, M. MoS_2 versatile spray-coating of 3D electrodes for the hydrogen evolution reaction. *Nanoscale* **2019**, *11*, 9888–9895. [CrossRef]
90. Ghosh, K.; Pumera, M. Free-standing electrochemically coated MoSx based 3D-printed nanocarbon electrode for solid-state supercapacitor application. *Nanoscale* **2021**, *13*, 5744–5756. [CrossRef]

91. Novcic, K.A.; Iffelsberger, C.; Ng, S.; Pumera, M. Local electrochemical activity of transition metal dichalcogenides and their heterojunctions on 3D-printed nanocarbon surfaces. *Nanoscale* **2021**, *13*, 5324–5332. [CrossRef] [PubMed]
92. Ghosh, K.; Pumera, M. MXene and MoS_3-x Coated 3D-Printed Hybrid Electrode for Solid-State Asymmetric Supercapacitor. *Small Methods* **2021**, *5*, 2100451. [CrossRef]
93. Wang, X.; Li, T.; Ma, H.; Zhai, D.; Jiang, C.; Chang, J.; Wang, J.; Wu, C. A 3D-printed scaffold with MoS_2 nanosheets for tumor therapy and tissue regeneration. *NPG Asia Mater.* **2017**, *9*, e376. [CrossRef]
94. Wang, H.; Zeng, X.; Pang, L.; Wang, H.; Lin, B.; Deng, Z.; Qi, E.L.X.; Miao, N.; Wang, D.; Huang, P.; et al. Integrative treatment of anti-tumor/bone repair by combination of MoS_2 nanosheets with 3D printed bioactive borosilicate glass scaffolds. *Chem. Eng. J.* **2020**, *396*, 125081. [CrossRef]
95. He, C.; Yu, L.; Yao, H.; Chen, Y.; Hao, Y. Combinatorial Photothermal 3D-Printing Scaffold and Checkpoint Blockade Inhibits Growth/Metastasis of Breast Cancer to Bone and Accelerates Osteogenesis. *Adv. Funct. Mater.* **2020**, *31*, 2006214. [CrossRef]
96. Anichini, C.; Czepa, W.; Pakulski, D.; Aliprandi, A.; Ciesielski, A.; Samorì, P. Chemical sensing with 2D materials. *Chem. Soc. Rev.* **2018**, *47*, 4860–4908. [CrossRef]
97. Zhang, Z.; Pan, P.; Liu, X.; Yang, Z.; Wei, J.; Wei, Z. 3D-copper oxide and copper oxide/few-layer graphene with screen printed nanosheet assembly for ultrasensitive non-enzymatic glucose sensing. *Mater. Chem. Phys.* **2017**, *187*, 28–38. [CrossRef]
98. Guo, Y.; Zhong, M.; Fang, Z.; Wan, P.; Yu, G. A Wearable Transient Pressure Sensor Made with MXene Nanosheets for Sensitive Broad-Range Human–Machine Interfacing. *Nano Lett.* **2019**, *19*, 1143–1150. [CrossRef]
99. Cheng, Y.; Ma, Y.; Li, L.; Zhu, M.; Yue, Y.; Liu, W.; Wang, L.; Jia, S.; Li, C.; Qi, T.; et al. Bioinspired Microspines for a High-Performance Spray Ti_3C_2Tx MXene-Based Piezoresistive Sensor. *ACS Nano* **2020**, *14*, 2145–2155. [CrossRef]
100. Wang, Z.; Gao, W.; Zhang, Q.; Zheng, K.; Xu, J.; Xu, W.; Shang, E.; Jiang, J.; Zhang, J.; Liu, Y. 3D-Printed Graphene/Polydimethylsiloxane Composites for Stretchable and Strain-Insensitive Temperature Sensors. *ACS Appl. Mater. Interfaces* **2019**, *11*, 1344–1352. [CrossRef]
101. Ding, H.; Wei, Y.; Wu, Z.; Tao, K.; Ding, M.; Xie, X.; Wu, J. Recent Advances in Gas and Humidity Sensors Based on 3D Structured and Porous Graphene and Its Derivatives. *ACS Mater. Lett.* **2020**, *2*, 1381–1411. [CrossRef]
102. Dua, V.; Surwade, S.P.; Ammu, S.; Agnihotra, S.R.; Jain, S.; Roberts, K.E.; Park, S.; Ruoff, R.S.; Manohar, S.K. All-Organic Vapor Sensor Using Inkjet-Printed Reduced Graphene Oxide. *Angew. Chem. Int. Ed.* **2010**, *49*, 2154–2157. [CrossRef]
103. Yasaei, P.; Behranginia, A.; Foroozan, T.; Asadi, M.; Kim, K.; Khalili-Araghi, F.; Salehi-Khojin, A. Stable and Selective Humidity Sensing Using Stacked Black Phosphorus Flakes. *ACS Nano* **2015**, *9*, 9898–9905. [CrossRef] [PubMed]
104. Hanlon, D.; Backes, C.; Doherty, E.; Cucinotta, C.S.; Berner, N.C.; Boland, C.; Lee, K.; Harvey, A.; Lynch, P.; Gholamvand, Z.; et al. Liquid exfoliation of solvent-stabilized few-layer black phosphorus for applications beyond electronics. *Nat. Commun.* **2015**, *6*, 8563. [CrossRef]
105. He, P.; Brent, J.R.; Ding, H.; Yang, J.; Lewis, D.J.; O'Brien, P.; Derby, B. Fully printed high performance humidity sensors based on two-dimensional materials. *Nanoscale* **2018**, *10*, 5599–5606. [CrossRef] [PubMed]
106. Kim, J.H.; Chang, W.S.; Kim, D.; Yang, J.R.; Han, J.T.; Lee, G.-W.; Kim, J.T.; Seol, S.K. 3D Printing of Reduced Graphene Oxide Nanowires. *Adv. Mater.* **2015**, *27*, 157–161. [CrossRef] [PubMed]
107. Zhang, Q.; Zhang, F.; Xu, X.; Zhou, C.; Lin, D. Three-Dimensional Printing Hollow Polymer Template-Mediated Graphene Lattices with Tailorable Architectures and Multifunctional Properties. *ACS Nano* **2018**, *12*, 1096–1106. [CrossRef]
108. Yao, Y.; Tolentino, L.; Yang, Z.; Song, X.; Zhang, W.; Chen, Y.; Wong, C.-P. High-Concentration Aqueous Dispersions of MoS_2. *Adv. Funct. Mater.* **2013**, *23*, 3577–3583. [CrossRef]
109. Casiraghi, C.; Macucci, M.; Parvez, K.; Worsley, R.; Shin, Y.; Bronte, F.; Borri, C.; Paggi, M.; Fiori, G. Inkjet printed 2D-crystal based strain gauges on paper. *Carbon* **2018**, *129*, 462–467. [CrossRef]
110. An, B.; Ma, Y.; Li, W.; Su, M.; Li, F.; Song, Y. Three-dimensional multi-recognition flexible wearable sensor via graphene aerogel printing. *Chem. Commun.* **2016**, *52*, 10948–10951. [CrossRef]
111. Jabari, E.; Ahmed, F.; Liravi, F.; Secor, E.B.; Lin, L.; Toyserkani, E. 2D printing of graphene: A review. *2D Mater.* **2019**, *6*, 042004. [CrossRef]
112. Shi, G.; Lowe, S.E.; Teo, A.J.T.; Dinh, T.K.; Tan, S.H.; Qin, J.; Zhang, Y.; Zhong, Y.L.; Zhao, H. A versatile PDMS submicrobead/graphene oxide nanocomposite ink for the direct ink writing of wearable micron-scale tactile sensors. *Appl. Mater. Today* **2019**, *16*, 482–492. [CrossRef]
113. Wang, Z.; Zhang, Q.; Yue, Y.; Xu, J.; Xu, W.; Sun, X.; Chen, Y.; Jiang, J.; Liu, Y. 3D printed graphene/polydimethylsiloxane composite for stretchable strain sensor with tunable sensitivity. *Nanotechnology* **2019**, *30*, 345501. [CrossRef] [PubMed]
114. Guo, F.; Jiang, Y.; Xu, Z.; Xiao, Y.; Fang, B.; Liu, Y.; Gao, W.; Zhao, P.; Wang, H.; Gao, C. Highly stretchable carbon aerogels. *Nat. Commun.* **2018**, *9*, 881. [CrossRef] [PubMed]
115. Sreenilayam, S.P.; Ul Ahad, I.; Nicolosi, V.; Brabazon, D. MXene materials based printed flexible devices for healthcare, biomedical and energy storage applications. *Mater. Today* **2021**, *43*, 99–131. [CrossRef]
116. Pandey, A.; Nikam, A.N.; Fernandes, G.; Kulkarni, S.; Padya, B.S.; Prassl, R.; Das, S.; Joseph, A.; Deshmukh, P.K.; Patil, P.O.; et al. Black Phosphorus as Multifaceted Advanced Material Nanoplatforms for Potential Biomedical Applications. *Nanomaterials* **2021**, *11*, 13. [CrossRef]
117. Athukorala, S.S.; Tran, T.S.; Balu, R.; Truong, V.K.; Chapman, J.; Dutta, N.K.; Roy Choudhury, N. 3D Printable Electrically Conductive Hydrogel Scaffolds for Biomedical Applications: A Review. *Polymers* **2021**, *13*, 474. [CrossRef]

118. Liu, X.; Miller, A.L.; Park, S.; George, M.N.; Waletzki, B.E.; Xu, H.; Terzic, A.; Lu, L. Two-Dimensional Black Phosphorus and Graphene Oxide Nanosheets Synergistically Enhance Cell Proliferation and Osteogenesis on 3D Printed Scaffolds. *ACS Appl. Mater. Interfaces* **2019**, *11*, 23558–23572. [CrossRef]
119. Palmieri, V.; Lattanzi, W.; Perini, G.; Augello, A.; Papi, M.; De Spirito, M. 3D-printed graphene for bone reconstruction. *2D Mater.* **2020**, *7*, 022004. [CrossRef]
120. Jakus, A.E.; Shah, R.N. Multi and mixed 3D-printing of graphene-hydroxyapatite hybrid materials for complex tissue engineering. *J. Biomed. Mater. Res.* **2017**, *105*, 274–283. [CrossRef]
121. Cheng, Z.; Xigong, L.; Weiyi, D.; Jingen, H.; Shuo, W.; Xiangjin, L.; Junsong, W. Potential use of 3D-printed graphene oxide scaffold for construction of the cartilage layer. *J. Nanobiotechnol.* **2020**, *18*, 97. [CrossRef]
122. Olate-Moya, F.; Arens, L.; Wilhelm, M.; Mateos-Timoneda, M.A.; Engel, E.; Palza, H. Chondroinductive Alginate-Based Hydrogels Having Graphene Oxide for 3D Printed Scaffold Fabrication. *ACS Appl. Mater. Interfaces* **2020**, *12*, 4343–4357. [CrossRef] [PubMed]
123. Peng, J.; Li, L.; Nie, Y.; Liu, T.; Song, K. 3D Bio-Printing Fabrication and Properties of Graphene Dispersion-based Hybrid Scaffolds. *J. Phys. Conf. Ser.* **2020**, *1622*, 012062. [CrossRef]
124. Lu, R.; Zhang, W.; He, Y.; Zhang, S.; Fu, Q.; Pang, Y.; Sun, W. Ferric ion crosslinking-based 3D printing of a graphene oxide hydrogel and its evaluation as a bio-scaffold in tissue engineering. *Biotechnol. Bioeng.* **2021**, *118*, 1006–1012. [CrossRef] [PubMed]
125. Kumar, A.; Venkatappa Rao, T.; Ray Chowdhury, S.; Ramana Reddy, S.V.S. Compatibility confirmation and refinement of thermal and mechanical properties of poly(lactic acid)/poly (ethylene-co-glycidyl methacrylate) blend reinforced by hexagonal boron nitride. *React. Funct. Polym.* **2017**, *117*, 1–9. [CrossRef]
126. Ciofani, G.; Raffa, V.; Menciassi, A.; Cuschieri, A. Boron nitride nanotubes: An innovative tool for nanomedicine. *Nano Today* **2009**, *4*, 8–10. [CrossRef]
127. Golberg, D.; Bando, Y.; Huang, Y.; Terao, T.; Mitome, M.; Tang, C.; Zhi, C. Boron Nitride Nanotubes and Nanosheets. *ACS Nano* **2010**, *4*, 2979–2993. [CrossRef] [PubMed]
128. Aki, D.; Ulag, S.; Unal, S.; Sengor, M.; Ekren, N.; Lin, C.-C.; Yılmazer, H.; Ustundag, C.B.; Kalaskar, D.M.; Gunduz, O. 3D printing of PVA/hexagonal boron nitride/bacterial cellulose composite scaffolds for bone tissue engineering. *Mater. Des.* **2020**, *196*, 109094. [CrossRef]
129. Li, R.; Lin, J.; Fang, Y.; Yu, C.; Zhang, J.; Xue, Y.; Liu, Z.; Zhang, J.; Tang, C.; Huang, Y. Porous boron nitride nanofibers/PVA hydrogels with improved mechanical property and thermal stability. *Ceram. Int.* **2018**, *44*, 22439–22444. [CrossRef]
130. Belaid, H.; Nagarajan, S.; Barou, C.; Huon, V.; Bares, J.; Balme, S.; Miele, P.; Cornu, D.; Cavaillès, V.; Teyssier, C.; et al. Boron Nitride Based Nanobiocomposites: Design by 3D Printing for Bone Tissue Engineering. *ACS Appl. Bio Mater.* **2020**, *3*, 1865–1874. [CrossRef]
131. Tang, D.; Tare, R.S.; Yang, L.-Y.; Williams, D.F.; Ou, K.-L.; Oreffo, R.O.C. Biofabrication of bone tissue: Approaches, challenges and translation for bone regeneration. *Biomaterials* **2016**, *83*, 363–382. [CrossRef]
132. Tao, W.; Zhu, X.; Yu, X.; Zeng, X.; Xiao, Q.; Zhang, X.; Ji, X.; Wang, X.; Shi, J.; Zhang, H.; et al. Black Phosphorus Nanosheets as a Robust Delivery Platform for Cancer Theranostics. *Adv. Mater.* **2017**, *29*, 1603276. [CrossRef] [PubMed]
133. Huang, K.; Wu, J.; Gu, Z. Black Phosphorus Hydrogel Scaffolds Enhance Bone Regeneration via a Sustained Supply of Calcium-Free Phosphorus. *ACS Appl. Mater. Interfaces* **2019**, *11*, 2908–2916. [CrossRef] [PubMed]
134. Wang, S.; Weng, J.; Fu, X.; Lin, J.; Fan, W.; Lu, N.; Qu, J.; Chen, S.; Wang, T.; Huang, P. Black Phosphorus Nanosheets for Mild Hyperthermia-Enhanced Chemotherapy and Chemo-Photothermal Combination Therapy. *Nanotheranostics* **2017**, *1*, 208–216. [CrossRef]
135. Zhang, X.; Chen, G.; Liu, Y.; Sun, L.; Sun, L.; Zhao, Y. Black Phosphorus-Loaded Separable Microneedles as Responsive Oxygen Delivery Carriers for Wound Healing. *ACS Nano* **2020**, *14*, 5901–5908. [CrossRef] [PubMed]
136. Xie, H.; Shao, J.; Ma, Y.; Wang, J.; Huang, H.; Yang, N.; Wang, H.; Ruan, C.; Luo, Y.; Wang, Q.-Q.; et al. Biodegradable near-infrared-photoresponsive shape memory implants based on black phosphorus nanofillers. *Biomaterials* **2018**, *164*, 11–21. [CrossRef]
137. Li, Z.; Du, T.; Ruan, C.; Niu, X. Bioinspired mineralized collagen scaffolds for bone tissue engineering. *Bioact. Mater.* **2021**, *6*, 1491–1511. [CrossRef]
138. Yang, B.; Yin, J.; Chen, Y.; Pan, S.; Yao, H.; Gao, Y.; Shi, J. 2D-Black-Phosphorus-Reinforced 3D-Printed Scaffolds: A Stepwise Countermeasure for Osteosarcoma. *Adv. Mater.* **2018**, *30*, 1705611. [CrossRef]
139. Wang, C.; Ye, X.; Zhao, Y.; Bai, L.; He, Z.; Tong, Q.; Xie, X.; Zhu, H.; Cai, D.; Zhou, Y.; et al. Cryogenic 3D printing of porous scaffolds for in situ delivery of 2D black phosphorus nanosheets, doxorubicin hydrochloride and osteogenic peptide for treating tumor resection-induced bone defects. *Biofabrication* **2020**, *12*, 035004. [CrossRef]
140. Anju, S.; Mohanan, P.V. Biomedical applications of transition metal dichalcogenides (TMDCs). *Synth. Met.* **2021**, *271*, 116610. [CrossRef]
141. Liu, Y.; Li, T.; Ma, H.; Zhai, D.; Deng, C.; Wang, J.; Zhuo, S.; Chang, J.; Wu, C. 3D-printed scaffolds with bioactive elements-induced photothermal effect for bone tumor therapy. *Acta Biomater.* **2018**, *73*, 531–546. [CrossRef]
142. Pan, S.; Yin, J.; Yu, L.; Zhang, C.; Zhu, Y.; Gao, Y.; Chen, Y. 2D MXene-Integrated 3D-Printing Scaffolds for Augmented Osteosarcoma Phototherapy and Accelerated Tissue Reconstruction. *Adv. Sci.* **2020**, *7*, 1901511. [CrossRef] [PubMed]
143. Yin, J.; Pan, S.; Guo, X.; Gao, Y.; Zhu, D.; Yang, Q.; Gao, J.; Zhang, C.; Chen, Y. Nb_2C MXene-Functionalized Scaffolds Enables Osteosarcoma Phototherapy and Angiogenesis/Osteogenesis of Bone Defects. *Nano-Micro Lett.* **2021**, *13*, 30. [CrossRef]
144. Li, Q.; Zheng, S.; Du, M.; Pang, H. Ultrathin nanosheet metal–organic framework@NiO/Ni nanorod composites. *Chem. Eng. J.* **2021**, *417*, 129201. [CrossRef]
145. Li, W.; Guo, X.; Geng, P.; Du, M.; Jing, Q.; Chen, X.; Zhang, G.; Li, H.; Xu, Q.; Braunstein, P.; et al. Rational Design and General Synthesis of Multimetallic Metal–Organic Framework Nano-Octahedra for Enhanced Li–S Battery. *Adv. Mater.* **2021**, 2105163. [CrossRef]

146. Zheng, S.; Ru, Y.; Xue, H.; Pang, H. Fluorinated pillared-layer metal-organic framework microrods for improved electrochemical cycling stability. *Chin. Chem. Lett.* **2021**, 6353. [CrossRef]
147. Hyun, W.J.; Secor, E.B.; Kim, C.-H.; Hersam, M.C.; Francis, L.F.; Frisbie, C.D. Scalable, Self-Aligned Printing of Flexible Graphene Micro-Supercapacitors. *Adv. Energy Mater.* **2017**, *7*, 1700285. [CrossRef]
148. Le, L.T.; Ervin, M.H.; Qiu, H.; Fuchs, B.E.; Lee, W.Y. Graphene supercapacitor electrodes fabricated by inkjet printing and thermal reduction of graphene oxide. *Electrochem. Commun.* **2011**, *13*, 355–358. [CrossRef]
149. Hyun, W.J.; Secor, E.B.; Hersam, M.C.; Frisbie, C.D.; Francis, L.F. High-Resolution Patterning of Graphene by Screen Printing with a Silicon Stencil for Highly Flexible Printed Electronics. *Adv. Mater.* **2015**, *27*, 109–115. [CrossRef] [PubMed]
150. Mensing, J.P.; Lomas, T.; Tuantranont, A. 2D and 3D printing for graphene based supercapacitors and batteries: A review. *Sustain. Mater. Technol.* **2020**, *25*, e00190. [CrossRef]
151. Abdelkader, A.M.; Karim, N.; Vallés, C.; Afroj, S.; Novoselov, K.S.; Yeates, S.G. Ultraflexible and robust graphene supercapacitors printed on textiles for wearable electronics applications. *2D Mater.* **2017**, *4*, 035016. [CrossRef]
152. Lin, Y.; Liu, F.; Casano, G.; Bhavsar, R.; Kinloch, I.A.; Derby, B. Pristine Graphene Aerogels by Room-Temperature Freeze Gelation. *Adv. Mater.* **2016**, *28*, 7993–8000. [CrossRef] [PubMed]
153. Zhu, C.; Liu, T.; Qian, F.; Han, T.Y.-J.; Duoss, E.B.; Kuntz, J.D.; Spadaccini, C.M.; Worsley, M.A.; Li, Y. Supercapacitors Based on Three-Dimensional Hierarchical Graphene Aerogels with Periodic Macropores. *Nano Lett.* **2016**, *16*, 3448–3456. [CrossRef]
154. Egorov, V.; Gulzar, U.; Zhang, Y.; Breen, S.; O'Dwyer, C. Evolution of 3D Printing Methods and Materials for Electrochemical Energy Storage. *Adv. Mater.* **2020**, *32*, 2000556. [CrossRef] [PubMed]
155. Rocha, V.G.; García-Tuñón, E.; Botas, C.; Markoulidis, F.; Feilden, E.; D'Elia, E.; Ni, N.; Shaffer, M.; Saiz, E. Multimaterial 3D Printing of Graphene-Based Electrodes for Electrochemical Energy Storage Using Thermoresponsive Inks. *ACS Appl. Mater. Interfaces* **2017**, *9*, 37136–37145. [CrossRef] [PubMed]
156. Peng, Y.-Y.; Akuzum, B.; Kurra, N.; Zhao, M.-Q.; Alhabeb, M.; Anasori, B.; Kumbur, E.C.; Alshareef, H.N.; Ger, M.-D.; Gogotsi, Y. All-MXene (2D titanium carbide) solid-state microsupercapacitors for on-chip energy storage. *Energy Environ. Sci* **2016**, *9*, 2847–2854. [CrossRef]
157. Yang, W.; Yang, J.; Byun, J.J.; Moissinac, F.P.; Xu, J.; Haigh, S.J.; Domingos, M.; Bissett, M.A.; Dryfe, R.A.W.; Barg, S. 3D Printing of Freestanding MXene Architectures for Current-Collector-Free Supercapacitors. *Adv. Mater.* **2019**, *31*, 1902725. [CrossRef] [PubMed]
158. Redondo, E.; Pumera, M. MXene-functionalised 3D-printed electrodes for electrochemical capacitors. *Electrochem. Commun.* **2021**, *124*, 106920. [CrossRef]
159. Briggs, N.; Subramanian, S.; Lin, Z.; Li, X.; Zhang, X.; Zhang, K.; Xiao, K.; Geohegan, D.; Wallace, R.; Chen, L.-Q.; et al. A roadmap for electronic grade 2D materials. *2D Mater.* **2019**, *6*, 022001. [CrossRef]
160. Yang, R.; Zhou, J.; Yang, C.; Qiu, L.; Cheng, H. Recent Progress in 3D Printing of 2D Material-Based Macrostructures. *Adv. Mater. Technol.* **2020**, *5*, 1901066. [CrossRef]
161. Jakus, A.E.; Secor, E.B.; Rutz, A.L.; Jordan, S.W.; Hersam, M.C.; Shah, R.N. Three-Dimensional Printing of High-Content Graphene Scaffolds for Electronic and Biomedical Applications. *ACS Nano* **2015**, *9*, 4636–4648. [CrossRef]
162. Seo, J.-W.T.; Zhu, J.; Sangwan, V.K.; Secor, E.B.; Wallace, S.G.; Hersam, M.C. Fully Inkjet-Printed, Mechanically Flexible MoS_2 Nanosheet Photodetectors. *ACS Appl. Mater. Interfaces* **2019**, *11*, 5675–5681. [CrossRef] [PubMed]
163. Wang, Z.; Kim, H.; Alshareef, H.N. Oxide Thin-Film Electronics using All-MXene Electrical Contacts. *Adv. Mater.* **2018**, *30*, 1706656. [CrossRef]
164. Jiang, X.; Li, W.; Hai, T.; Yue, R.; Chen, Z.; Lao, C.; Ge, Y.; Xie, G.; Wen, Q.; Zhang, H. Inkjet-printed MXene micro-scale devices for integrated broadband ultrafast photonics. *NPJ 2D Mater. Appl.* **2019**, *3*, 34. [CrossRef]
165. Chaudhuri, K.; Alhabeb, M.; Wang, Z.; Shalaev, V.M.; Gogotsi, Y.; Boltasseva, A. Highly Broadband Absorber Using Plasmonic Titanium Carbide (MXene). *ACS Photonics* **2018**, *5*, 1115–1122. [CrossRef]
166. Joseph, A.M.; Nagendra, B.; Bhoje Gowd, E.; Surendran, K.P. Screen-Printable Electronic Ink of Ultrathin Boron Nitride Nanosheets. *ACS Omega* **2016**, *1*, 1220–1228. [CrossRef] [PubMed]
167. Guo, Q.; Pospischil, A.; Bhuiyan, M.; Jiang, H.; Tian, H.; Farmer, D.; Deng, B.; Li, C.; Han, S.-J.; Wang, H.; et al. Black Phosphorus Mid-Infrared Photodetectors with High Gain. *Nano Lett.* **2016**, *16*, 4648–4655. [CrossRef] [PubMed]
168. Castellanos-Gomez, A. Nanomanufacturing: There's Still Plenty of Room at the Bottom. *Nanomanufacturing* **2021**, *1*, 1–2. [CrossRef]